1-1-2013

Plant Virus Based Materials For Cell Alignment and Differentiation

Elizabeth Balizan
University of South Carolina

PLANT VIRUS BASED MATERIALS FOR CELL ALIGNMENT AND DIFFERENTIATION

by

Elizabeth Balizan

Bachelor of Arts
New Mexico Highlands University, 2006

Submitted in Partial Fulfillment of the Requirements

For the Degree of Doctor of Philosophy in

Chemistry and Biochemistry

College of Arts and Sciences

University of South Carolina

2013

Accepted by:

Qian Wang, Major Professor

Stephen Kistler, Committee Member

Lukasz Lebioda, Committee Member

Rekha Patel, Committee Member

Lacy Ford, Vice Provost and Dean of Graduate Studies

ACKNOWLEDGEMENTS

No words spoken or written here do justice to the following people or their importance. First, I would like to thank my husband Wassim Basheer for all his support not only in this but in all aspects of my life. Also, I would like to thank my mentor, Qian Wang. He has given me opportunities I only dreamed of and taught me about the beauty of science. In addition, I would like to thank my family for their pride and support. Everyone should be as lucky as I am. Furthermore, I would like to thank all members of the Wang lab. It is from them I have learned about the exquisiteness of the world.

ABSTRACT

This research focused on developing and using plant virus based scaffolds to understand substrate control over cell alignment and differentiation. The first part of this work centered on development of virus based patterns that were then used to align and elongate aortic smooth muscle cells (SMCs). Virus patterns were generated in capillary tubes via a simple drying method. Three experimental parameters were used to control pattern formation: (1) protein concentration, (2) salt concentration, and (3) hydrophobicity of the pre-deposition surface. By controlling these parameters several aspects of the final virus patterns were controlled. First, virus orientation was controlled. Patterns were made that had rod like virus particles oriented either parallel or perpendicular to the long axis of the capillary tube. Second, patterns were formed that either had a monolayer or multilayer (5 layers) of virus. Finally, virus coverage was controlled. Stripe patterns were formed with different widths of virus stripes and different widths of spacing between virus stripes. Different pattern formations were generated by (1) interfacial assembly of tobacco mosaic virus (TMV) at the air/liquid interface and (2) a pinning-depinning process. These patterns were then used to investigate SMC morphology, elongation, alignment, and differentiation. Our data indicates that the virus based stripe patterns could control SMC morphology and induce the elongation and alignment of SMCs. However, no effect on SMC differentiation was observed.

The second part of this work focused on the use of genetically mutated viruses as substrates to support and improve the differentiation of mesenchymal stem cells (MSCs). The virus surfaces were created by coating high protein binding plates with genetically mutated viruses. These tobacco mosaic virus mutants display selected peptide fragments reported to bind integrin receptors or selected sequences derived from other integrin binding matrix proteins. Differentiation of MSCs into osteoblasts was monitored for 21 days. The differentiation was monitored through alkaline phosphatase activity, calcium quantification, and ELISA quantification of osteopontin and osteocalcin, two important biomarkers for osteogenesis. Experimental evidences generated by cytochemical staining and ELISA showed that certain mutant substrates supported differentiation of MSCs. Furthermore, substrates made of mutant viruses with multivalent RGD displays decreased the time to onset of mineralization.

The third part of this work combined a method for creating ordered virus patterns with the use of mutant TMV particles to create substrates that could both align and differentiate neuroblast and myoblast cells. Specifically, a flow assembly method was used to align either native or mutant TMV particles. The experimental parameters used to control virus alignment and density included: flow rate, virus concentration, salt concentration, and charge of the pre-deposition surface. These aligned virus patterns were then used as substrates to control cell growth. It was found that virus density and alignment played significant roles in the final orientation and differentiation of myoblasts and neuroblasts.

Collectively the research presented in this dissertation used the unique qualities of virus particles to create cell substrates that can align different cell types or modulate the

differentiation of different cell types. These substrates may be used in the future to gain more insight into substrate based control over cell alignment and differentiation.

TABLE OF CONTENTS

LIST OF FIGURES

INTRODUCTION

Virus materials

Plant viruses are monodisperse particles with organized three-dimensional architecture and can be isolated in high yields and purities [1, 2]. The many varieties are diverse in shape (including rods and spheres) and size (from tens to hundreds of nanometers). The highly ordered spatial arrangement of their coat proteins allow them to be used as scaffolds for polyvalent display of functional groups in many applications [3, 4]. In fact the distinctive properties of plant viruses have allowed them to be used in materials for electronics, drug delivery, imaging, gene therapy, and immunotherapy [3, 5-13]

Tobacco mosaic virus (TMV)

This work employed tobacco mosaic virus (TMV). It is a plant virus with helical symmetry and rod-like structure. Native TMV is composed of a single strand of RNA and 2130 identical coat protein subunits. The coat protein subunits assemble around the RNA to form a 300 × 18 nm tubular structure. TMV was ideal for these studies because it is:

Easily obtainable: TMV and its mutants can be harvested from infected plants following a simple and well established protocol [14, 15].

Stable: TMV can withstand wide ranges of pH (3.5-9.0), temperature (up to 90^{o}C), salinity, and solvents (including ethanol and dimethylsulfoxide) [15-17].

Structurally well defined: TMV has been resolved using X-ray crystallography allowing angstrom resolution of each amino acid residue on the coat protein [18].

Genetically and chemically modifiable: TMV modification (both genetic and chemical) can be done in wide variety and has been well documented [15, 19, 20].

Monodisperse: TMV has little particle size variation which is superb for creating highly ordered nanoparticle assemblies.

Cell Response

Substrates are known to affect many cellular processes such as morphology, proliferation, differentiation, migration or apoptosis [21-23]. The general size range of eukaryotic cells is tens to hundreds of micrometers; however, cell sensing, signaling, and interaction all occur in the nanometer range [24].

A cell's natural environment is very complex. Many features of a cells natural environment play a role in cell response. Features such as ligand density, and spatial arrangement [23, 25, 26]. However, only limited methodologies are available to engineer a biomaterial surface with desired functionalities that influence different cellular functions [23, 27-29]. It is difficult to build scaffolds from naturally derived biopolymers such as elastin and collagen [23]. Maintaining the quality and activity of harvested biopolymers throughout their extraction, processing, and remodeling is challenging. Therefore, it is necessary to create synthetic materials that incorporate features similar to the cell's natural environment such as ligand distance, density, and spatial arrangement.

The research here focused on creating and employing surfaces designed to study cellular alignment and differentiation. In the first chapter we employed the unique stability and monodispersity of TMV to create ordered virus patterns that aligned and elongated SMCs. In the second chapter we used genetically modified TMV to create substrates that supported differentiation of MSCs. In the last chapter we used genetically modified TMV to create aligned virus substrates that induced both alignment and differentiation of myoblast and neuroblast cells.

CHAPTER 1

SELF-ASSEMBLED VIRUS PATTERNS INDUCE SMOOTH MUSCLE CELL ALIGNMENT

1.1 ABSTRACT

This chapter centered on development of virus based patterns that were then used for alignment and elongation of aortic smooth muscle cells (SMCs). Virus patterns were generated in capillary tubes via a simple drying method. Three experimental parameters were used to control pattern formation: (1) protein concentration, (2) salt concentration, and (3) hydrophobicity of the pre-deposition surface. By controlling these parameters several aspects of the final virus patterns were controlled. First, virus orientation was controlled. Patterns were made that had rod like virus particles oriented either parallel or perpendicular to the long axis of the capillary tube. Second, the number of virus layers in the pattern was controlled. Patterns were formed that either had a monolayer or multilayer (5 layers) of virus. Finally, virus coverage was controlled. Stripe patterns were formed with different widths of virus stripes and different widths of spacing between virus stripes. Two processes governed the formation of different patterns during the assembly: (1) interfacial assembly of TMV at the air/liquid interface, and (2) a pinning-depinning process. These patterns were then used to investigate SMC morphology, elongation, alignment, and differentiation. Our data indicates that the virus based stripe

patterns could control SMC morphology and induce elongation and alignment. However, there was no effect on SMC differentiation.

1.2 INTRODUCTION

Smooth muscle cells

SMCs were selected as the prototypical cell for this study because: (1) Alignment is important for the proper function of SMCs; (2) SMC differentiation plays a role in several diseases including atherosclerotic disease; and (3) SMC differentiation can be guided by external extracellular forces.

Alignment is important for the proper function of SMCs. In the blood vessel SMCs align circumferentially. Contraction and relaxation allows them to control luminal diameter. This maintains proper blood pressure and blood flow distribution. This in turn is important in several physiological processes i.e. exercise, pregnancy, injury, and inflammation [30, 31].

Second, the differentiation and phenotypic switching of smooth muscle cells (SMCs), from contractile into synthetic morphology or vice versa, is recognized as a key in a number of major human diseases particularly atherosclerosis, [32] the number one killer of Americans today [33].

Third, SMC differentiation is known to be affected by the extracellular environment. The SMC is surrounded by a complex extracellular matrix that provides and modulates a variety of biochemical and mechanical cues that guide cell function. New materials that can create complex in vitro culture environments will lead to a better understanding of SMC biology and new treatments for vascular disease [34].

Material formation

The alignment of nanoparticle building blocks into ordered hierarchical structures is very important in colloidal and materials chemistry [35]. Self-assembly of nanoparticle suspensions is a relatively easy method that is used to fabricate large-scale patterns with well-defined superstructures [36]. The formation of a ringlike structure at the contact line when a suspension dries on a solid surface is an everyday phenomenon that has been widely used to create hierarchical patterned structures [37]. The contact line can stay pinned to form a single ring (i.e., "coffee ring") [38] or can shrink in a discontinuous manner to generate multiple rings [39]. This phenomenon can be used to tune the formation of different patterns in a confined geometry [40, 41]. Basic theoretical studies have been performed to understand how different patterns are formed during the drying process [38]. In general, the pinning and depinning process (also termed as "stick–slip motion") at the contact line governs such pattern formation [42]. Spherical colloidal particle suspensions and polymer solutions are two widely used systems for theoretical and experimental studies. A systematic study of the orientation of anisotropic particles, such as nanorods, at the contact line during the drying process can further improve the theoretical understanding of pattern formation induced by solvent evaporation. From a practical point of view, such knowledge may lead to a facile method of patterning and alignment of rodlike particles, which is critical for applications such as thin-film transistors, molecular electronics, and biosensors [43-48].

Tobacco mosaic virus

TMV is an ideal candidate for these studies because of its rodlike morphology, high monodispersity and stability. TMV has also been widely used as a model rodlike particle in self-assembly studies [49] and a basic building block for new materials development [50]. In addition, TMV has also been shown to improve differentiation of mesenchymal stem cells [27, 51, 52]. Therefore we hypothesize that it is possible to use TMV to make ordered patterns that can affect the alignment and differentiation of stem cells.

1.3 MATERIALS AND METHODS

1.3.1 Materials

TMV was isolated according to previously reported methods [53]. The salts in the TMV solution were removed by several rounds of dialysis against deionized, ultrapure water. Poly(diallyldimethylammonium chloride) (PDDA) (Mw 100,000~200,000), poly(styrenesulfonic acid) (PSS) (Mw = 70,000), sodium dodecyl sulfate (SDS), paraformaldehyde (P6148) and bovine serum albumin (BSA) (≥ 98% pure by gel electrophoresis) were purchased from Sigma–Aldrich Co. All the chemicals were used as received without further purification. Ultrapure water was obtained from Millipore Synergy UV system (18.2 MΩ). Powder media (Dulbecco's Modification of Eagle's Medium/Ham's F-12 50/50 Mix), was purchased from Mediatech Incorporated's Cellgro 90-090-PB. Fetal bovine serum (FBS) was purchased from Atlanta Biologicals (catalog # S12450, lot # G0059). L-glutamine and penicillin-streptomycin were purchased from Invitrogen (catalog numbers 25030081 and 15140122 respectively). Sodium bicarbonate (S233-500), sodium chloride (S271-500), potassium chloride (Mallinckrodt 6858),

sodium phosphate (S374-500), potassium phosphate monobasic (P285-500), and hydrochloric acid (A481-212) were all purchased from Fisher Scientific. FITC conjugated phalloidin (ALX-350-268-MC01) was purchased from Alexis Biochemicals. Upon arrival it was dissolved in methanol resulting in an 8.0 × 10 µM stock solution and stored at -20^{o} C. Cell culture dishes were purchased from Corning via Fisher (catalog # 430641.) Trypsin was purchased from Invitrogen (catalog # 2500056). Incubator used was from Sheldon Labs Model 2375. Glass slides were purchased from Fisher (catalog # 12-550-A3). Borosilicate glass capillary tubes (inner diameter 0.15 cm then cut to length of 2.0 cm) were purchased from KIMBLE Co. Hemacytometer from Fisher (0267110). Filters (0.2 µm) were used from Pall Corporation (4454). BSA was received from VWR (RLBSA50).

1.3.2 Solutions

Serum free cell media was prepared by adding 5.85 g powder media, 0.60 g $NaHCO_3$, 7.0 mL L-glutamine solution, and 5 mL penicillin-streptomycin to 500 mL water. The solution was then vacuum filtered using a large 0.2 µm filter. Cell media was prepared as serum free media with the addition of 50 mL FBS before filtration. Fixation solution was prepared by adding 10 g paraformaldehyde to 250 mL of 65^{o} C PBS. Solution was kept at 65^{o} C and stirred for 4 hours. Then a few drops of 0.1 M NaOH was added to the solution until a pH of 7 was reached. This was then stored at 4^{o} C. A 0.1% (v:v) solution of Triton X-100 was made by mixing 100 µL of Triton X-100 with 100 mL PBS. This was stored at room temperature. A 1% (m:v) solution of BSA was made by adding 1 g of BSA to 100 mL of PBS. This was stored at 4^{o} C.

1.3.3 Fabrication of protein patterns

Cylindrical capillaries glass tubes form KIMBLE Co. with an inner diameter of 1.5 mm were cleaned by piranha solution (7:3 mixture of 98% H_2SO_4 and 30% H_2O_2) at 75 ℃ for 2 h. These were stored under water or ethanol until use. To provide a systematic range of contact angle of surfaces, the surfaces of the blank glass tubes were modified via the layer-by-layer method. The cleaned glass tubes were submerged in the PDDA (1 mg/mL) solution for 1 h to allow for complete coverage of the substrate surfaces, then washed thoroughly with ultrapure water and dried with N_2 gas. Subsequently submerged the positively charged surface to the solution of PSS (2 mg/mL) or PSS:SDS (1:5) for 20 min, then washed thoroughly with ultrapure water and dried with N_2 gas. The negatively charged surface is indicated as glass/PSS (PSS layer was coated as the outermost surface) and glass/PSS:SDS (PSS:SDS layer was coated as the outermost surface). Directly before patterning tubes and slides were rinsed with water and dried thoroughly with N_2 gas. Tubes were then secured to a flat surface with double sided tape. TMV solution (25 μL) was injected into the cleaned glass tubes and surface modified tubes. After which, the tubes were maintained in the horizontal position on the flat bench at room temperature and 40~60 % humidity. All the samples were ready after three days. Glass slides were laid on a flat bench top and separated by glass spacers. Then 1.5 mL of 0.1 mg/mL TMV solution was injected between the slides and allowed to dry under the same conditions as the glass capillary. Glass slides and capillary tubes were then stored (in non-sterile polystyrene dishes, ambient conditions, up to 1 month) or used directly in cell culture experiments. Directly before cell culture experiments tubes were cut in half to give 1 cm tubes. Both tubes and slides were then rinsed with water, special care was taken to

thoroughly rinse the inside of the tubes. Then, tubes and slides were moved to cell culture cabinet, rinsed (inside and out) with water, then ethanol, and stuck to the bottom of a sterile cell culture plates (12 well) by a bead of sterile silicone grease (tubes) or laid in square culture dishes (slides).

1.3.4 SMC sub-culture

After initial SMC culture was established SMCs were sub-cultured by washing nearly confluent plates (~85%) with PBS twice, 0.04 mL/cm^2. Then 0.013 mL/cm^2 trypsin was added to plates and let stand 60 seconds. Then 0.04 mL/cm^2 of media was added to the culture plates. Media was used to wash the cells from the surface. Cells were counted using hemacytometer and then inoculated at density of 3.3 thousand/cm^2 on a 75 cm^2 culture dish. Media added so that total volume was 0.13 mL/cm^2. Media was replaced every 48 hours. SMCs from sub-cultures 3-8 were used in experiments.

1.3.5 Cell viability

Cell viability was tested using Promega's Celltiter-Blue Cell Viability Assay (PR-G8080). SMCs were seeded in 96 well plate at a density of 50 k cell/mL and 100 µL/well, allowed to attach for 48 hours then media was replaced with TMV supplemented media at concentrations of 0.00 mg/mL, 0.005 mg/mL, 0.05 mg/mL, 0.1 mg/mL, or 1.0 mg/mL. Each solution concentration had 8 wells of replicates. SMCs were then allowed to grow for either 24 hours or 48 hours. Then 20 µL (20 µL/100 µL media) of CellTiter-Blue Reagent was added to each well. Cells were incubated for 2 hours and then 50 µL of 3% SDS was added to each well and plates were gently agitated for a few seconds and fluorescence was read within 30 minutes.

1.3.6 Elongation and orientation

SMCs were seeded on either piranha treated or protein patterned glass slide substrates. SMCs were seeded at a density of 3.3 thousand cell/cm^2. Final media volume was 0.13 mL/cm^2. SMCs were incubated for 24 hours and then fixed. Cells were fixed by: Gently washed cells 3× with PBS. Then added 0.26 mL/cm2 paraformaldehyde solution and let stand for 30 min. Washed 3× for 5 min each with warm or room temperature PBS. Last wash of PBS was left on cells. Cells were used directly for staining or stored in 4 ^{o}C until used (no longer than 1 week).

1.3.7 Fluorescent cell staining

Staining procedure: All solutions used in staining were at room temperature. Removed PBS wash/storage solution from fixed cell samples and then added 0.26 mL/cm^2 of TritonX100 solution. Let sit for 15 minutes and then removed TritonX100 solution. Washed samples 3 times with 0.26 mL/cm^2 PBS; let sit 5 minutes each wash. Added 0.26 mL/cm^2 1% BSA solution to samples and gave gentle rocking for 1 hour. Add antibodies/stains to give final concentrations of 1:500 FITC phallodin. Protect from light and gently rock for 1 hour. Wash 3× with PBS (vol/cm^2), 5 min for each wash. Mount: invert on glass slide with 5 µL DAPI mounting solution. Paint edges with nail polish. Protect from light and allow to dry 15 min.

1.3.8 Migration assay

Migration assays were set up similar to the elongation and orientation assays. However SMCs were seeded at density of 6.6 thousand cell/cm^2. After being allowed to attach for 24 hours SMCs were serum deprived for 24 hours. Substrates were then

scratched with a 10 pipette tip either perpendicular or parallel to the protein pattern. Substrates were then gently washed 2× with serum free media. Pictures of live cells were taken on an Olympus IX81 microscope operating in transmission mode. Plates were then incubated for 8, 12, 16, or 24 hours with either serum free or regular media and then imaged again.

1.3.9 mRNA analysis

Initial set up is similar to elongation and orientation assays. SMCs were cultured on substrates for 2, 4, 8, or 10 days. At these time points total RNA was extracted from cells using Qiagen RNeasy mini purification kits. RNA quantification and purity testing was done using a Bio-Rad Experion system and Experion RNA StdSens Analysis kits. RNA was then reverse transcribed using Quanta qScript cDNA SuperMix (84034). RT-qPCR was done using iQ SYBR Green Supermix and an iQ5 real-time PCR detection system from Bio-Rad laboratories. RT-qPCR details: 40 cycles of PCR (94^{o} C for 15 s, 55^{o} C for 30 s, and 70^{o} C for 10 s) after initial denaturation of 8 min and 45 s at 95^{o} C. For each reaction 5 µL of cDNA was added, final volume was 20 µL, and primers were at a concentration of 500 nM. Glyceraldehyde 3-phosphate dehydrogenase (GAPDH) was used as the housekeeping gene. Fluorescence data was collected for each cycle during the 70^{o} C step. Threshold cycle (C_T) values were determined using the iQ5 system software. Expression levels were calculated using C^T values for each sample. Triplicates of each sample type were analyzed and each of these was run in duplicate reactions.

1.4 RESULTS

1.4.1 Fabrication of protein patterns in tubes and on flat surfaces.

Protein patterns were easily obtained on both the convex curved surface of capillary tubes and the flat surface of glass slides (Figure1.1). Control over virus pattern formation was achieved by varying protein concentration, salt concentration, pH, and surface hydrophobicity. By manipulating these factors protein patterns were fine tuned to create a variety of topographies, including monolayers, multilayers, monolayer stripes, multilayer stripes, thin stripes, and wide stripes. Patterns of different proteins could also be assembled on other types of surfaces such as polydimethylsiloxane (PDMS) and quartz crystal. This technique can hence be applied to other types surfaces and other proteins or biomacromolecules which renders it great potential.

First studies were done on pattern formation from various concentrations of TMV at fixed salt concentration (0.01 $_{M}$ potassium phosphate buffer, pH 7.4; Figure 1.2). With a TMV concentration of 0.01 mg mL^{-1}, stripe patterns were formed around the interior of the capillary tube or on the internal side glass slide sandwich. Micrographs of the stripes taken by AFM clearly showed that the band is only composed of a single layer of TMV particles (Figure 1.2 a). The particles form a close packed structure, in which TMVs were oriented parallel to the contact line but perpendicular to the long axis of the capillary tube. Similar patterns were formed when the TMV concentration was increased to 0.1 mg mL^{-1} (Figure 1.2 b); each band was composed of multiple layers of TMV, which were also oriented parallel to the contact line. Upon further increasing the TMV concentration to 0.5 mg mL^{-1}, the entire capillary tube was covered with TMV, and no stripe patterns

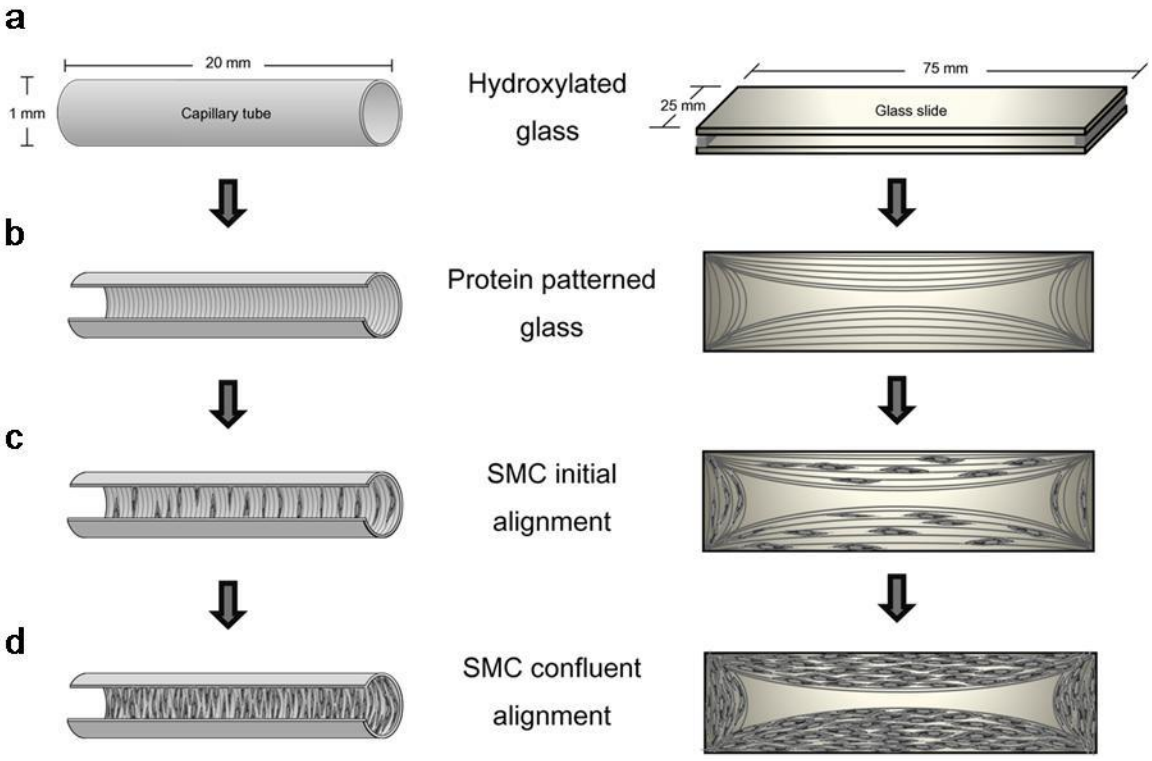

Figure 1.1 Schematic illustration of the fabrication process of substrates (left: glass capillary; right: glass slides). a) Glass capillary or slide is initially acid/peroxide treated to create a hydrophilic surface. b) A protein solution of specific ionic strength and pH is dried within the confined space of the substrates to create protein stripe patterns. c) Substrates are rinsed and seeded with SMCs. d) After several days incubation, SMC become confluent while maintaining alignment.

were observed, while most TMVs still aligned perpendicular to the long axis of the tube, although it was not a perfect pattern (Figure 1.2 c).

The TMV concentration determined the amount of particles supplied to the stripe-growing region, which was directly related to the width and thickness of the stripes. A higher concentration of the TMV solution drove more TMV particles to the tip of the meniscus, where the particle film grows, thus resulting in thicker and wider stripes. At higher concentrations of TMV (0.05 mg mL^{-1} < [TMV] < 0.5 mg mL^{-1}), a multilayer of TMV stripe patterns was formed. The width of the TMV stripes and adjacent spacing increased almost linearly against TMV concentration (Figure 1.3 a). At low TMV concentrations (0.01 mg mL^{-1} < [TMV] <0.05 mg mL^{-1}), monolayer stripes formed and the stripe width increased linearly against the particle concentration. However, all the monolayer samples had the same stripe thickness, which resulted in equal-sized meniscuses and thus equal-sized adjacent spacings (Figure 1.3 b).

If the salt was removed, the assembly behavior changed dramatically. Instead of stripes, irregular aggregations of TMV were formed in the capillary tube at a TMV concentration of 0.01 mg mL-1 in pure water (Figure 1.4 a). Without a salt in solution to screen the charges, the overall negatively charged TMV particles (the isoelectric point (pI) of TMV is 3.4) [50] repelled each other. As a result, when some TMV particles were deposited at the contact line, other virus particles were repelled. No regular patterns could be formed in this situation. At a TMV concentration of 0.1 mg mL-1, the air–liquid interface was saturated with randomly packed viral particles; therefore, TMV randomly deposited on the substrate and formed a loose multilayer structure (Figure 1.4 b). A further increase in the TMV concentration resulted in a continuous TMV thin film where

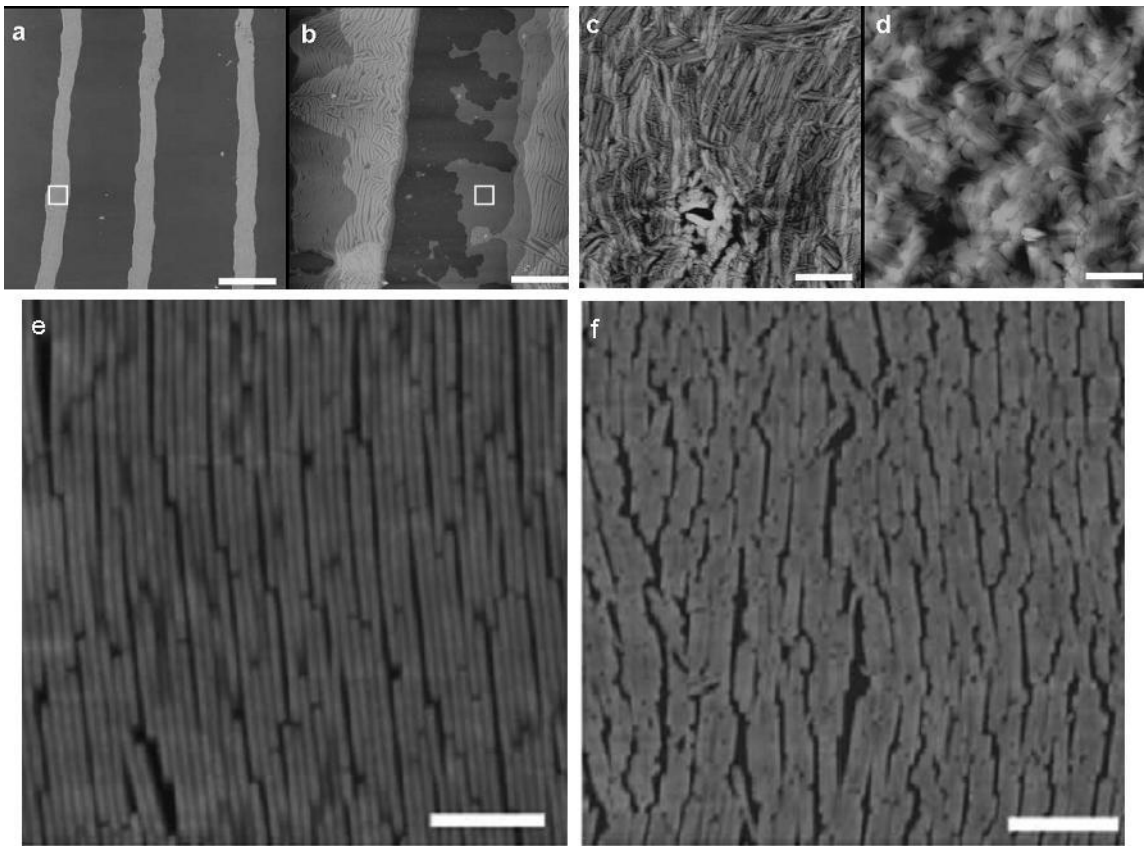

Figure 1.2 Patterns formed in glass capillary tube after evaporation of different concentrations of TMV in potassium phosphate buffer (0.01 M, pH 7.4). Concentrations of TMV: a, 0.01 mg/mL; b, 0.1 mg/mL; c, 0.5 mg/mL; d, 5 mg/mL. e and f) Enlarged views of the square regions enclosed by the white boxes in (a and b). Scale bars: a, 4 μm; b, 10 μm; c, 4 μm; d, 4 μm e, 200 nm; f, 400 nm.

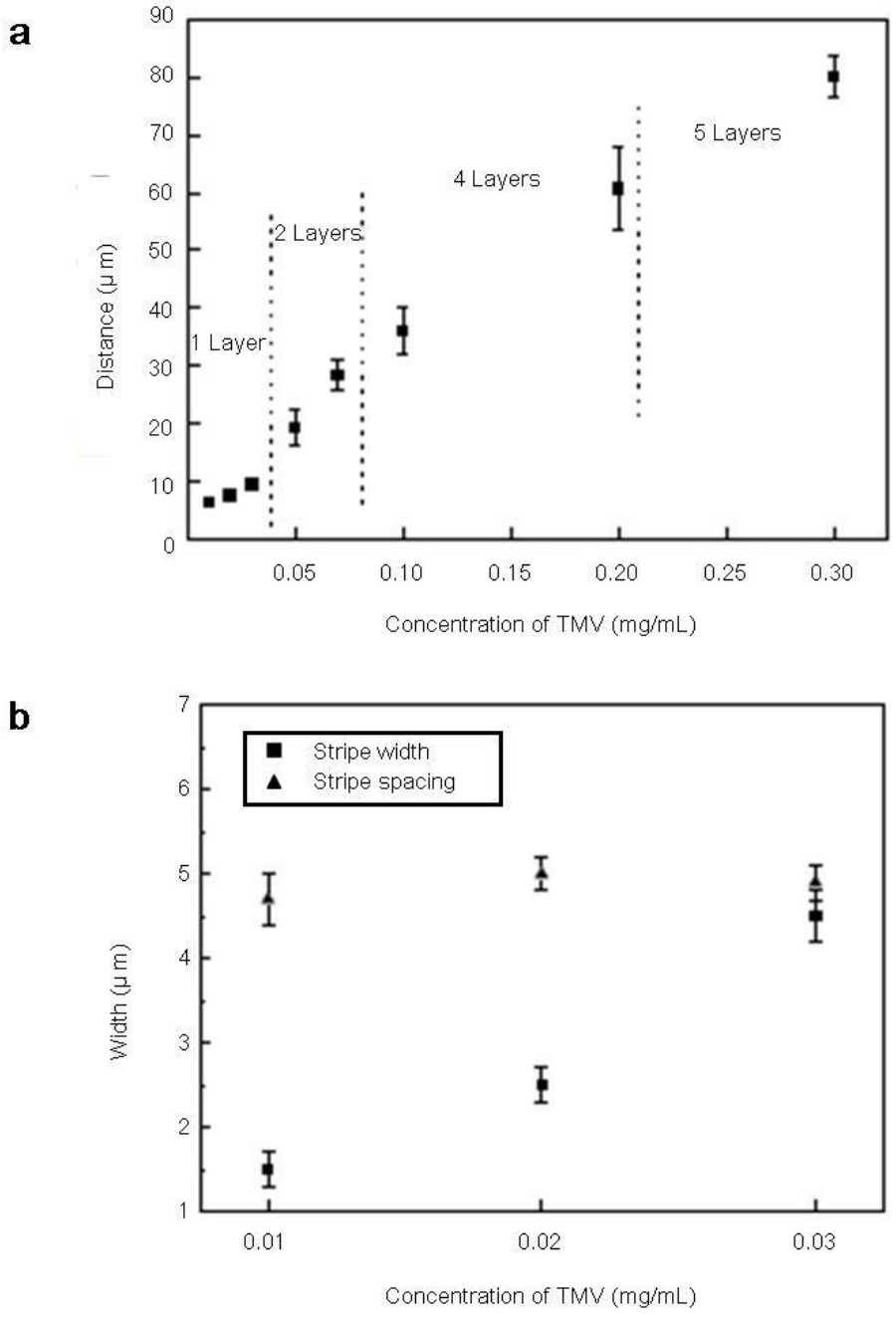

Figure 1.3 a) Stripe width plus adjacent spacing as a function of concentration of TMV in potassium phosphate buffer (0.01 M, pH 7.4). Error bars indicate the standard deviation of the data. b) Stripe width and adjacent spacing as a function of low concentration of TMV in potassium phosphate buffer (0.01 M, pH 7.4).

virus particles were oriented perpendicular to the contact line but parallel to the long axis of the capillary tube (Figure 1.4 c and d).

As well as the concentration and salt effects, the surface properties of the capillary interior surface played an important role in the pattern formation. In order to form a stripe pattern, the contact angle between water and the substrate must be smaller than the contact angle between water and TMV ($\theta_{tmv} = 40 \pm 3^o$). For example, the contact angle between water and clean glass θ_{glass} is 10 ± 3^o. To confirm this condition, two substrates, coated with PSS and a mixture of PSS/SDS (1:5) respectively, were prepared through a layer-by-layer method. TMV formed similar stripe patterns on the PSS-coated surface, which had a contact angle of 24 ± 2^o which is smaller than that of TMV. In comparison, on a PSS/SDS modified surface, which has a contact angle of 60 ± 2^o which is larger than that of TMV the contact line could not be pinned, and the capillary force drives TMV inside the tube. Most TMV was found in the middle part of the capillary tube (data not shown).

1.4.2 SMC response to virus orientation, layer thickness and stripe width

SMCs grown on virus stripe patterns aligned with the stripe patterns. They also tended to be spindle shaped, which is typical of the contractile phenotype (Figure 1.5 g, h). To determine the affect of virus stripe width, SMCs were grown on stripe patterns with various widths (Figure 1.5 g, h). It was found that the distance between SMC stripes correlated with the TMV stripe width (Figure 1.5 g, h). Furthermore, for SMCs in glass capillary tubes without TMV pattern (Figure 1.5 e), the morphology of SMCs was epithelioid or rhomboid, which is typical of the pathogenic synthetic phenotype [32]. In

addition, SMCs grown in glass capillary tubes with continuous coverage did not attach (Figure 1.5 f). This indicated that TMV coating blocked SMC attachment. This forced SMCs to attach and spread on the glass areas.

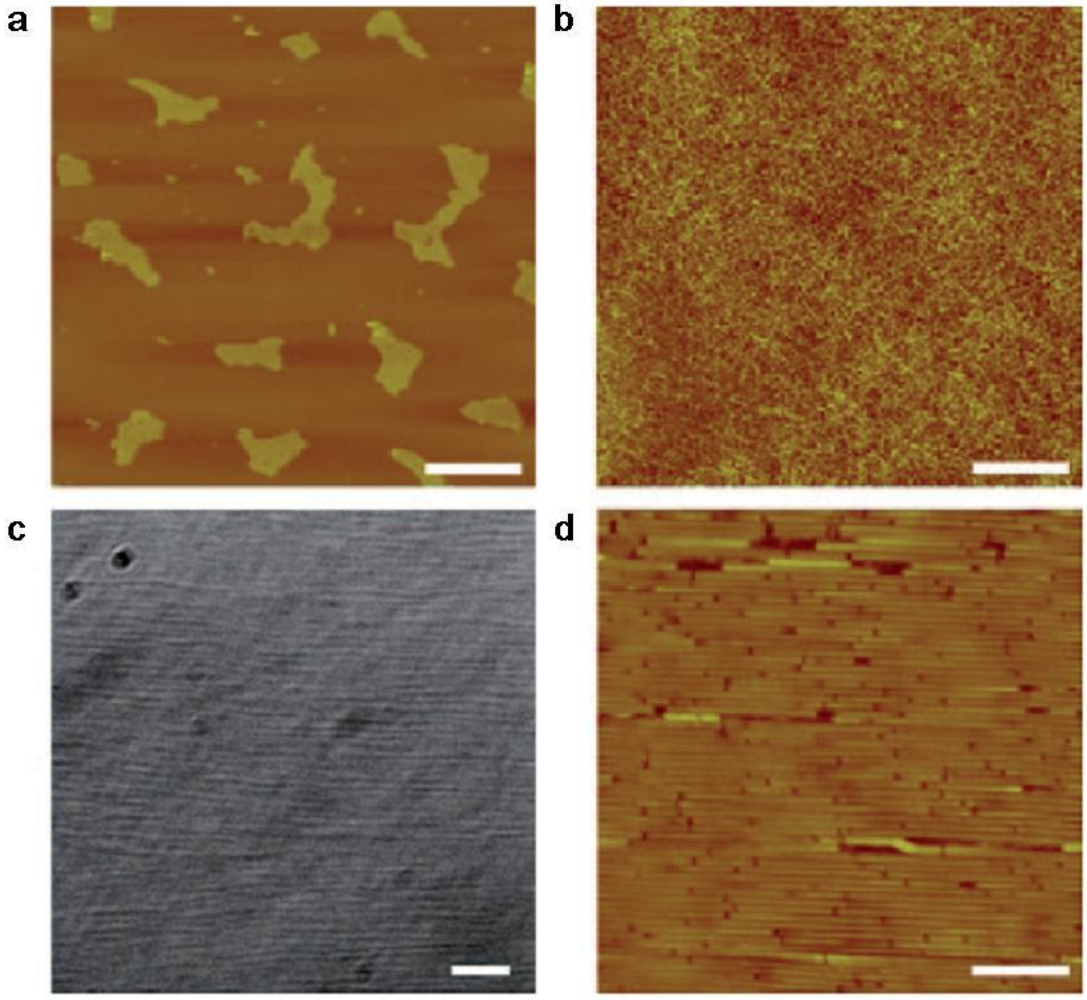

Figure 1.4 AFM images of drying TMV solution in capillary tubes without salt. TMV concentrations of a) 0.01 mg mL^{-1} and b) 0.1 mg mL^{-1}. c) Optical and d) AFM images of 26 mg mL^{-1}. Scale bars: a) and b) 4 mm; c) 10 mm; and d) 200 nm.

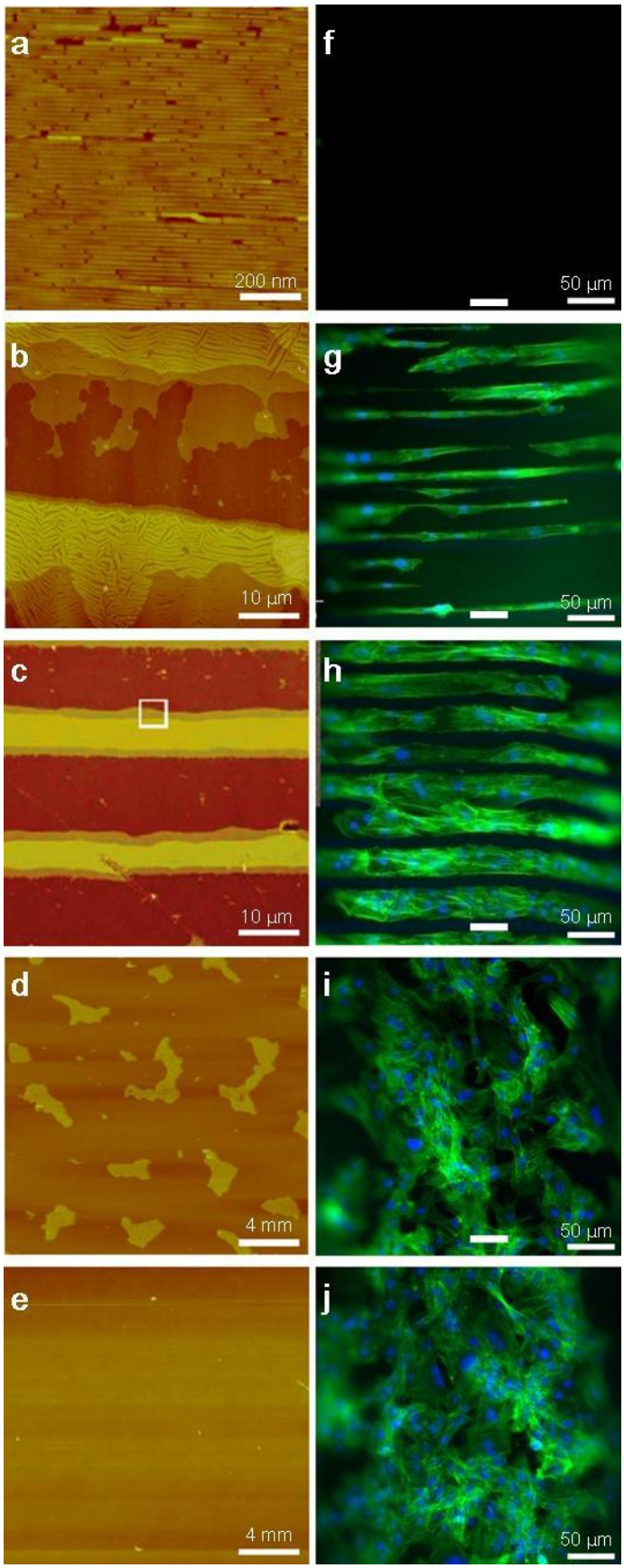

Figure 1.5 AFM images of various TMV patterns (a-e) and florescence images of SMCs on each type of virus pattern (f-j). Continuous TMV films (a and f) show no cell attachment. Wide stripe patterns with small adjacent spacing allow single file SMC attachment and alignment with wide gaps between cells (b and g). Thin stripe patterns with large adjacent spacing allows SMC attachment of many cells per stripe and small gaps between stripes (c and h). Irregular aggregations of TMV result in random SMC orientation and a synthetic phenotype (d and i). Plain glass substrates also result in random SMC orientation with a synthetic phenotype (e and j).

As controls, cells were seeded on stripe patterns made from different proteins, BSA or hFN (Figure 1.6). These proteins were chosen because of their ability to either block cell attachment (BSA) or improve cell attachment (hFN). When SMCs attached and spread on BSA stripe patterns they behaved similarly to those on TMV stripe patterns (Figure 1.6 a, c). Conversely when SMCs attached and spread on the hFN stripe patterns they behaved similarly to the SMCs on glass controls. They had no alignment and the morphology of SMCs was epithelioid or rhomboid (Figure 1.6 b and d). These results combined with our initial results indicated that both the TMV and BSA coatings blocked SMC attachment; whereas the hFN coating and the glass allowed attachment. These experiments not only indicated the mechanism through which TMV stripes control SMC morphology but also showed that this technique can be applied to other types of materials and other biomacromolecules.

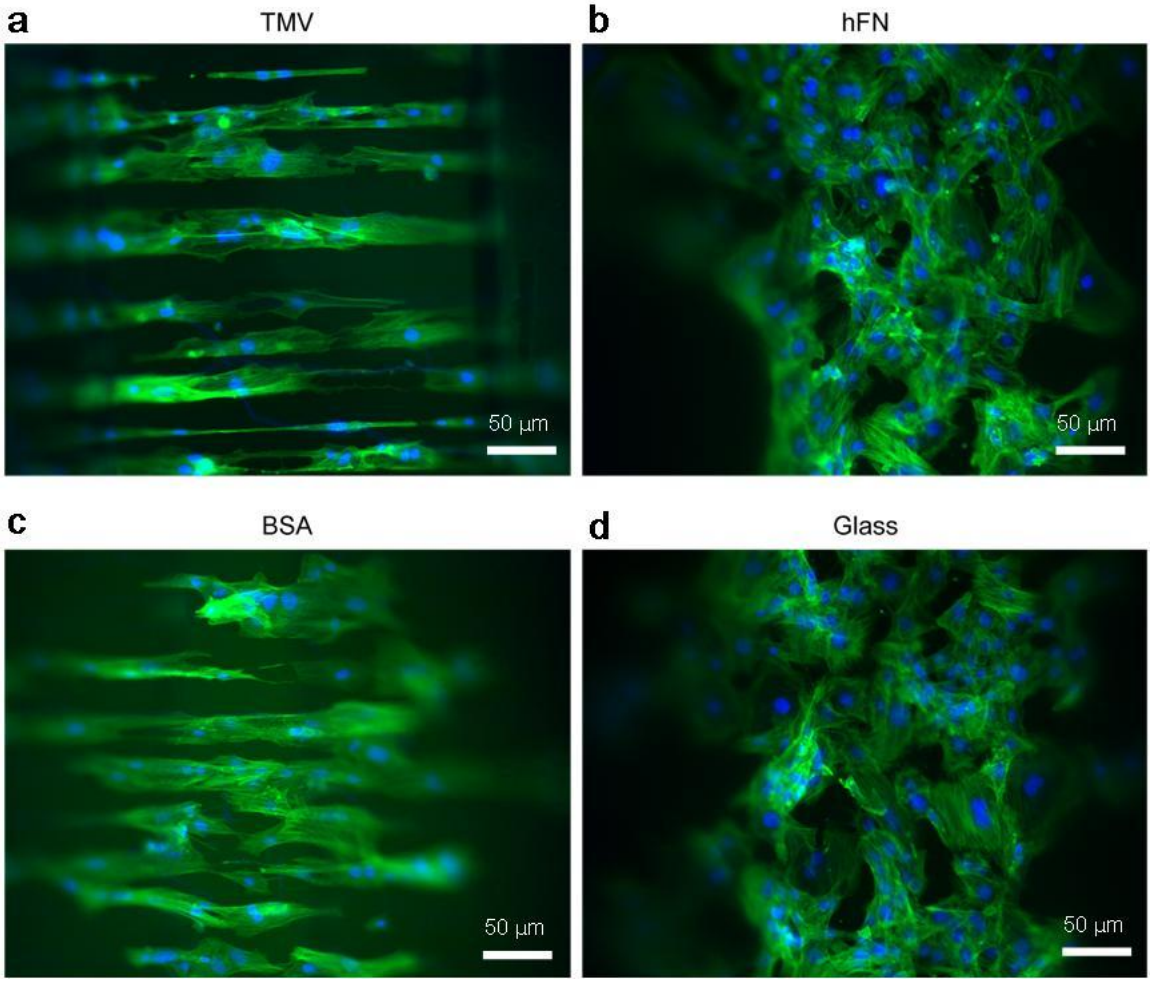

Figure 1.6 Florescence images of SMCs patterned inside the capillary tubes with different types of protein stripe patterns. Protein patterns made from a) TMV, b) hFN, c) BSA, and d) glass control.

1.4.3 Toxicity of TMV

Because SMCs did not attach to TMV stripes, it was necessary to test the cytotoxicity of TMV. To do this, SMCs were grown in media containing different concentrations of TMV. SMCs grown in TMV media showed no outward signs of stress. SMC morphology remained identical to untreated SMCs. Furthermore SMCs exposed to TMV solutions showed no significant change in their ability to reduce resazurin into resorufin (Figure 1.7). This lack of response of SMC to TMV in solution suggests that TMV does not affect cellular processes. Essentially TMV it is an inert protein to SMCs. Because of this "inertness" TMV can be used to block SMC attachment and spreading.

1.4.4 Orientation and elongation of SMC on stripe pattern

SMC grown on stripe patterns aligned in the direction of the pattern and did not align when grown on glass substrates. To quantify this, individual cell alignment was measured. Cell alignment angles were measured with respect to the stripes. SMCs on the stripe pattern showed a high degree of alignment, >80% had an orientation angle less than 5^{o}. Alternatively, less than 10% of SMCs grown on the non-patterned glass substrates exhibited an orientation angle less than 5% (Figure 1.8). Further investigation showed that actin filaments and nuclei also oriented with the stripe pattern (data not shown).

Once this initial alignment was established SMCs were allowed to proliferate and migrate onto all areas of the pattern. This gave rise to confluent sheets of aligned SMCs (day 7).

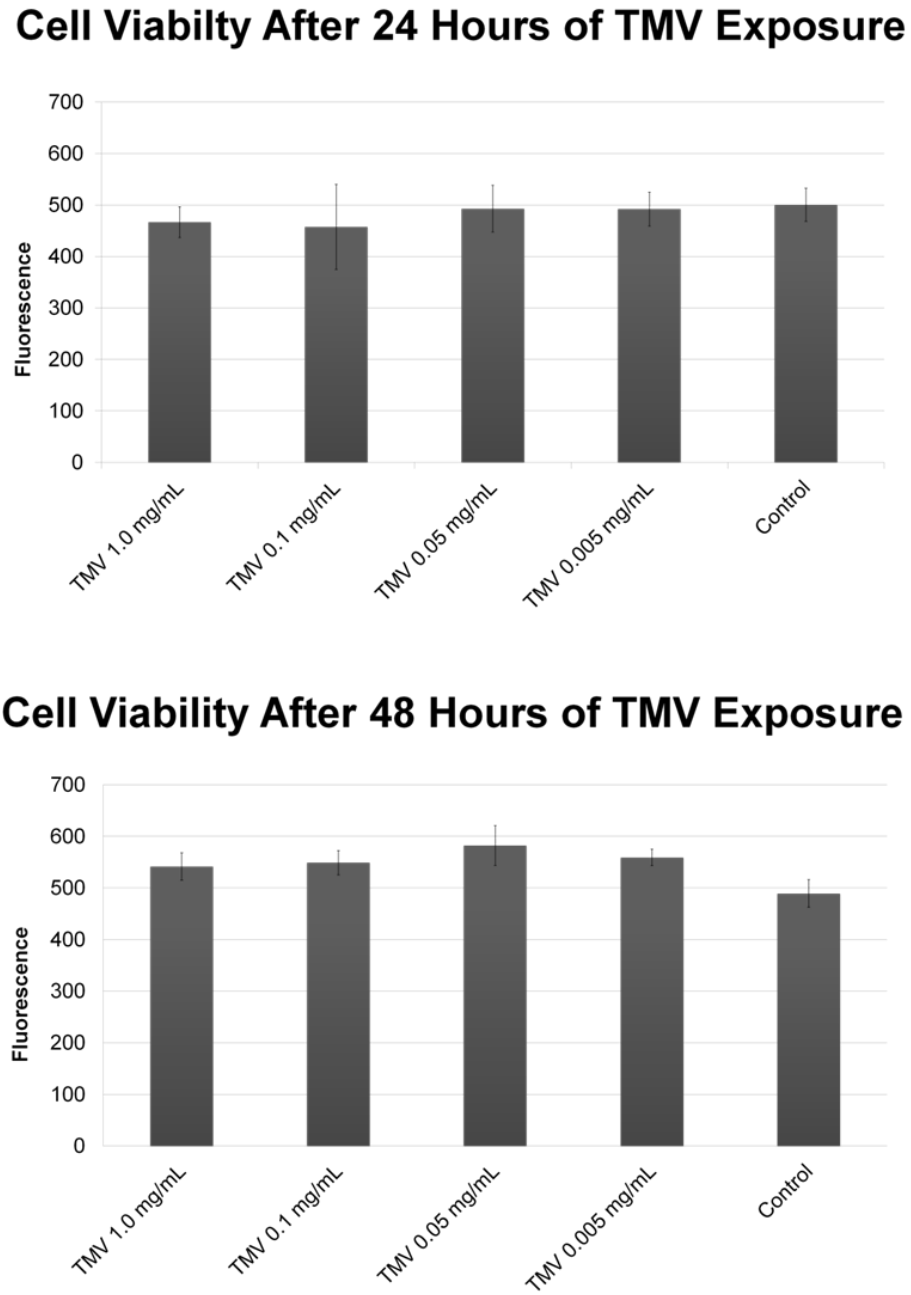

Figure 1.7 Smooth muscle cell ability to convert resazurin into resorufin. Cells were allowed to attach to cell culture plate (96 well) for 24 hours. Media was then changed to virus infused media. After 24 or 48 hours resazurin was added to wells for 2 hours. Eight replicate wells were measured for each sample type. Error bars correspond to mean ± standard deviation. No significant difference between the control and treated cells was obtained ($p > 0.05$) from paired student's t-test.

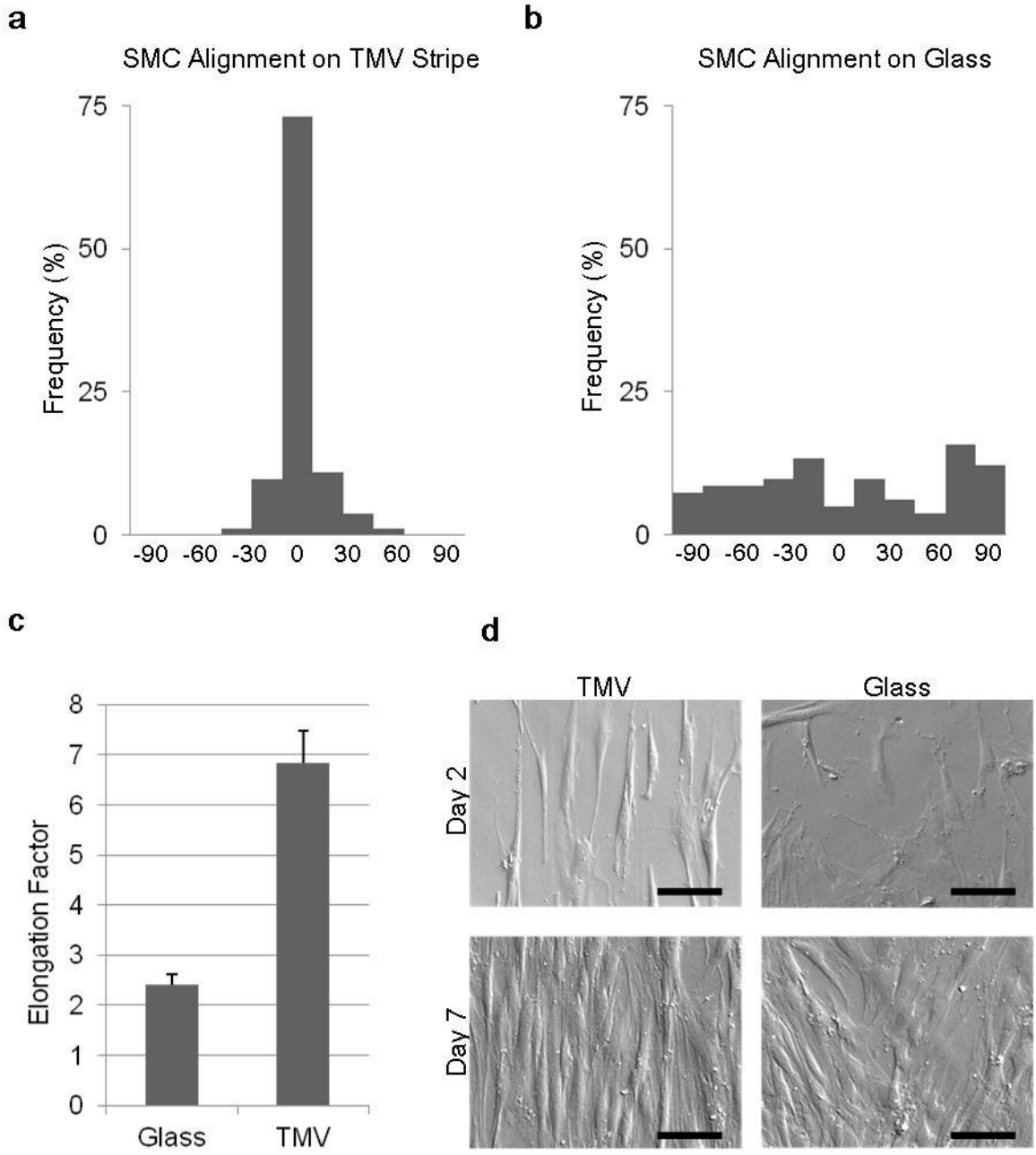

Figure 1.8 Alignment and elongation of SMCs. a) Alignment of SMCs on TMV stripe patterns and b) glass substrates. c) Elongation factor of SMCs on TMV stripe patterns and glass substrates. Elongation factor = (long axis/short axis) - 1. d) Confluent alignment of SMCs observed on TMV stripe patterns after 7 days. Scale bars are 50 μm. For alignment x-axis was set parallel to TMV stripe pattern and was arbitrarily set on glass.

Therefore SMCs were likely digesting the protein patterns or laying down their own extracellular matrix over the protein pattern that allowed them to spread over the pattern and achieve confluence.

1.4.5 Migration of SMC on stripe pattern.

SMC migration was measured using a scratch assay. This technique was used because it is one of the two widely accepted techniques for measuring SMC migration, but also is the only technique applicable to our system [54, 55]. Cells were seeded either on stripe patterns or on glass. After cells attached, cells were removed from a specific area via a scratch. Migration of SMCs from the surrounding areas into the scratch was monitored over a 24 hour period. Time points 8, 12, 16, and 24 hours were checked. However even after 24 hours no significant difference in the rate of migration was measured between SMCs on the stripe pattern vs. SMCs on glass (Figure 1.9). Furthermore, the ability of SMCs to migrate across the TMV stripe (cross TMV stripe) and along the TMV stripe (with TMV stripe) was measured. This was done by making scratches either parallel or perpendicular to the stripe pattern and monitoring SMC migration into these two types of scratches over a 24 hour period. After 24 hours no cells had migrated across the TMV stripe but many had migrated with the TMV stripe (Figure 1.9). This finding further supported the hypothesis that the TMV coating blocks the attachment of SMCs.

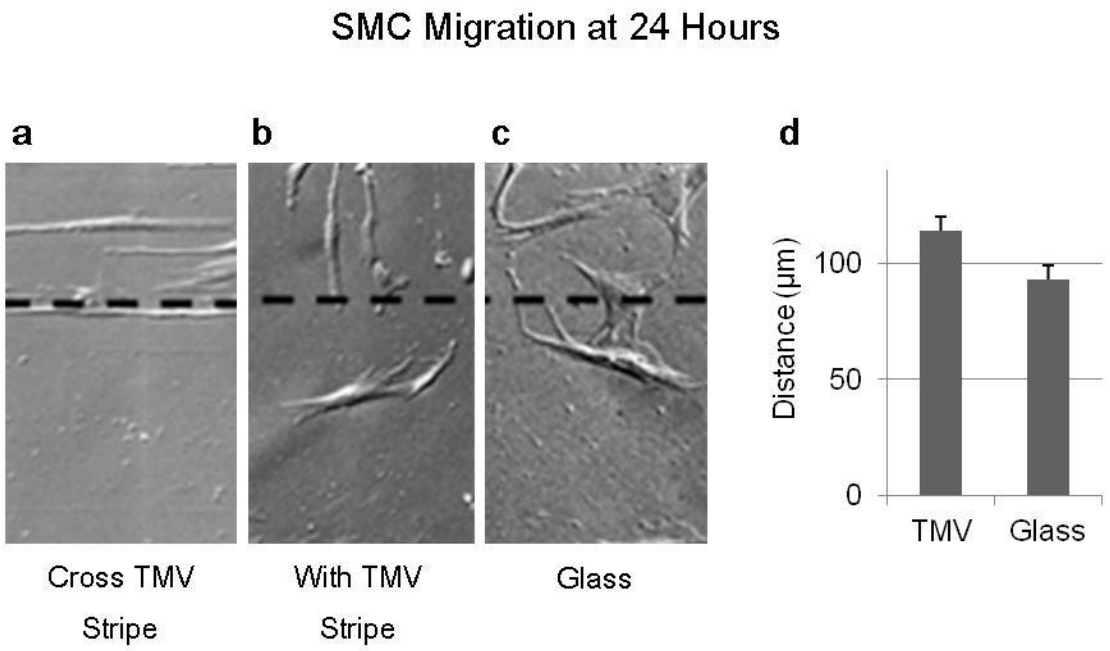

Figure 1.9 SMC migration. Migration into scratch was measured after 8, 12, 16, and 24 hours. No significant difference was found in migration distance of SMCs on TMV stripe patterns compared to glass control at any time point. However, it was found that SMCs could not migrate across TMV stripe patterns.

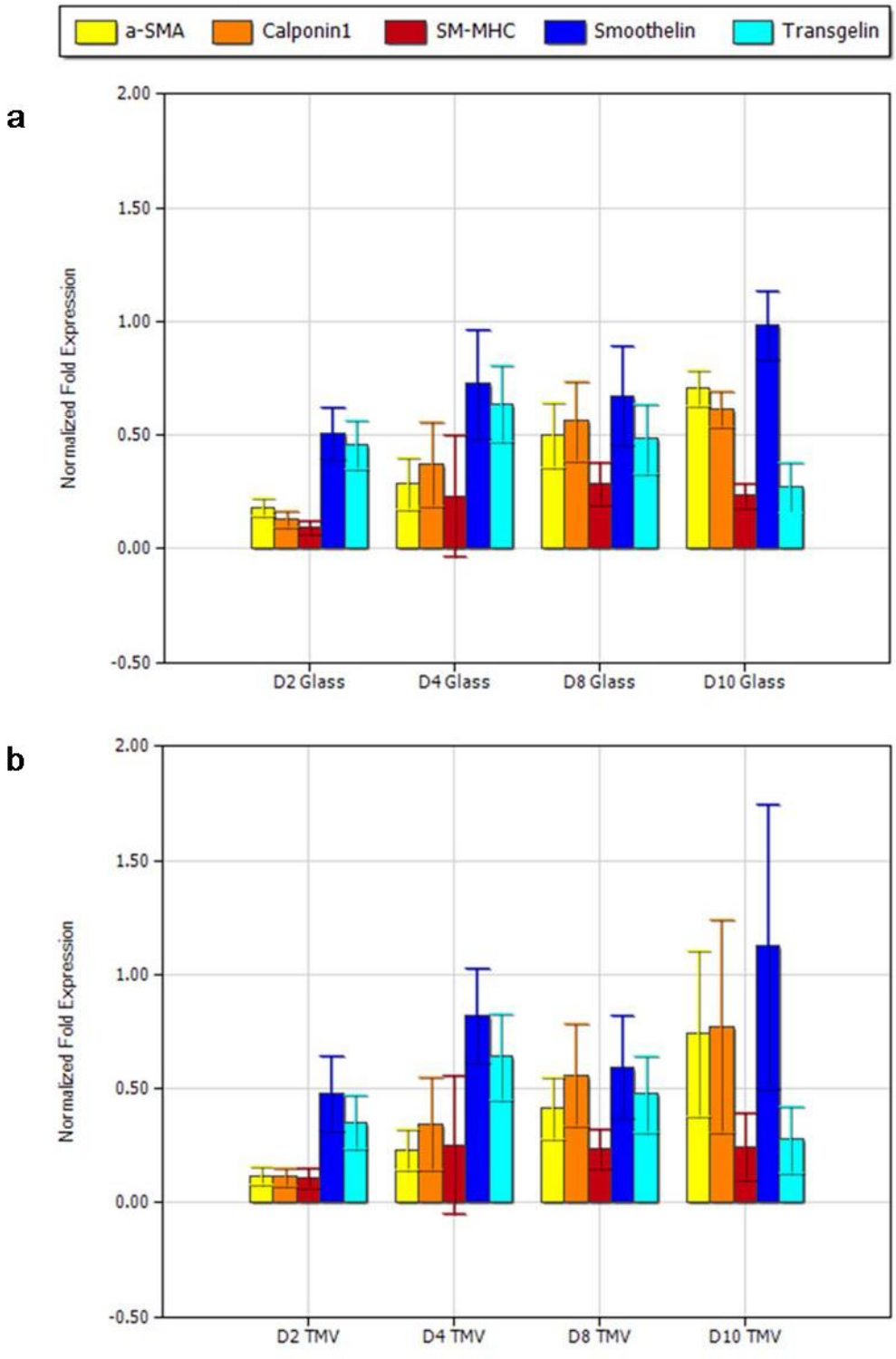

Figure 1.10 mRNA expression of SMC differentiation markers analyzed by RT-qPCR after growing cells on either a) glass control substrates or b) TMV stripe substrates. Expression normalized using *Gapdh* as the internal control. No significant difference between cells on TMV and glass substrates was obtained from 'pair wise fixed reallocation randomization test'.

1.4.6 mRNA results of SMC on stripe pattern.

The gene expression of SMCs on TMV stripes was monitored by real-time PCR. Five genes were examined: alpha smooth muscle actin (α-SMA), calponin1, smooth muscle myosin heavy chain (SM-MHC), smoothelin, and transgelin (SM22-α). Gene expression was determined over a 10 day period at days 2, 4, 8, and 10 (Figure 10). There was no significant change in gene expression when SMCs were grown on the TMV stripes.

These genes were chosen because they are most commonly used when determining the state of SMC differentiation-maturation[31, 32, 56]. A combination of genes was used because no one gene can definitively mark SMC phenotype. SM-MHC and α-SMA are smooth muscle isoforms of contractile proteins [31]. Calponin1 is a calcium binding and regulatory protein [32]. Smoothelin is a regulator of contraction and is widely used in determining SMC maturation because its expression is more uniformly and more rapidly downregulated in cultured vascular SMCs modulating towards a synthetic phenotype [31]. SM22-α is a calponin like protein associated with contractile function [57]. Calponin1, smoothelin, and SM22-α serve as late differentiation makers and are more abundant in spindle-shaped SMCs than in epithelioid and rhomboid SMC [56].

1.5 CONCLUSION

In this chapter, virus based patterns were created and then used for alignment and elongation of aortic smooth muscle cells. Patterns were obtained on both the convex curved surface of capillary tubes and the flat surface of glass slides. Pattern formation was controlled by protein concentration, salt concentration, and hydrophobicity of the pre-deposition surface. TMV concentration directly affected the width and thickness of

the pattern stripes. Removing salt from the high concentration virus solution resulted in a continuous TMV thin film where virus particles were oriented perpendicular to the contact line but parallel to the long axis of the capillary tube. Virus patterns could not be formed if the contact angle between water and the substrate was larger than the contact angle between water and TMV.

These patterns were then used to investigate SMC morphology, elongation, alignment, and differentiation. It was found that TMV stripe patterns induced alignment and elongation in SMCs. However, SMCs aligned and elongated on TMV stripe patterns but did not show any other signs of differentiation towards a contractile phenotype.

CHAPTER 2

VIRUS MUTANT SUPPORTED OSTEOGENIC DIFFERENTIATION OF MESENCHYMAL STEM CELL

2.1 ABSTRACT

This study focused on the use of genetically mutated viruses as substrates to support and improve the differentiation of mesenchymal stem cells (MSCs). Virus substrates were created by coating high protein binding plates with genetically mutated viruses. These tobacco mosaic virus (TMV) mutants display selected peptide fragments reported to bind integrin receptors or partial sequences derived from other integrin binding matrix proteins. Differentiation of MSCs was monitored through alkaline phosphatase activity, calcium quantification, and ELISA quantification of osteopontin and osteocalcin. MSCs on these substrates were monitored for 21 days. Experimental evidence generated by cytochemical staining and ELISA showed that mutant virus substrates supported the differentiation of MSCs. Furthermore, substrates made of mutant viruses with multivalent RGD displays decreased the time to onset of mineralization. This was an improvement over TMV substrates. Finally, it was shown that MSCs could undergo differentiation on substrates coated with the coat proteins of mutated TMV.

2.2 INTRODUCTION

Developing novel substrates/materials is essential, in the cell world, to understand cellular responses to environment. Cells are naturally responsive to their substrates/physical environment and there are a multitude of responses cells can exhibit ranging from migration to differentiation to apoptosis. *In vivo*, the ECM is distinctive at different stages of development and also in different tissues. This is possible through the different combinations and geometrical arrangements of collagens, elastins, proteoglycans, and adhesion proteins [23]. The work here uses mutated plant viruses as substrates to study the differentiation pathway of MSCs into osteoblasts.

TMV was chosen to do this work because it tolerates mutations and can have biologically relevant sequences inserted into its coat protein subunits. The site of modification was based on previous reports of TMV tolerating large inserts near its carboxy region [58]. The amino acid sequences were selected based on peptide fragments reported to bind integrin receptors or partial sequences derived from other integrin binding matrix proteins (i.e. collagen, vitronectin, fibronectin, and integrin-binding sialoprotein) with sequences ranging from 4 amino acids to 15 amino acids. Previous work has shown that the inserts of different peptides affect cell attachment and spreading differently and can be used as reliable cell culture substrates to investigate ECM effects on cell processes [59].

In addition, TMV was chosen because its native state has been shown to support and promote osteogenic differentiation of MSCs [51]. MSCs grown on substrates coated with the native TMV exhibited earlier expression of osteogenic markers over a 21 day time course. These MSCs formed fully mineralized nodules and structures comprising of

osteoblast-like cells around 14 days. This was compared to MSCs on tissue culture plastic, which did not show fully mineralized nodules until day 21. Additional experimental evidence generated by real time quantitative PCR (qPCR) analyses. DNA microarrays and immunohistochemistry/cytochemical staining further corroborated these findings [51]. This faster differentiation of MSCs on native TMV particles shows that native TMV, as a substrate, supports osteogenic differentiation of MSCs, and can induce an early onset of mineralization by seven days.

Finally, TMV and its mutants were chosen for this group of studies because of their stability, supramolecular assembly, high monodispersity and modifiability. The inherent supramolecular assembly of virus particles gives rise to very precise displays of the chosen ligands in the mutant viruses. Its rodlike morphology, high monodispersity and stability makes it ideal for use in a facile method for creating highly ordered protein patterns. For simplicity this chapter only employed non patterned virus mutants. This was to separate the effect of ligand display from topographical virus patterning. In the next chapter we used both topographical virus patterns and mutant viruses to control cell attachment, spreading, and differentiation.

The work in this chapter focuses on understanding cellular responses, specifically differentiation, of MSCs. MSCs were chosen because they are adult stem cells with the ability to differentiate into various phenotypes. These adult stem cells can be harvested from bone marrow and have the unique ability of self-renewal [60-62]. They can be expanded *in vitro* and then differentiated into many cell types [63, 64], including osteoblasts [65], chondrocytes [66, 67], and adipocytes [68]. Much is known about the

soluble factors that are capable of inducing differentiation in these cells. However, little is known about the role scaffolds play in this differentiation.

2.3 MATERIALS AND METHODS

2.3.1 Media

Serum media, DMEM high glucose, was made by adding 6.7 g powder media (Hyclone, SH30003.03), 1.2 g sodium bicarbonate (Fisher Scientific , S233-500), 3.57 g HEPES (Cellgro, 61-034-RM), 5.0 mL L-glutamine solution (Invitrogen, 25030081), and 5 mL penicillin-streptomycin (Invitrogen, 15140122) to 500 mL water (Millipore Synergy UV system, 18.2 MΩ). The solution was then brought to pH 7.4 using 1 M sodium hydroxide solution (J.T. Baker, E31H10). The media was sterilized by vacuum filtration using a low protein binding media filter (Corning 0.22 µm, 431097). Finally, 50 mL of fetal bovine serum (FBS) was added (Atlanta Biologicals, S12450).

Serum free osteogenic media base was made similar to serum media, however, without FBS. To finish the serum free osteogenic media 10 nm dexamethazone (VWR, 89157-624), 50 µg/mL ascorbic acid (Sigma, A8960-5G), 10 mM β-glycerolphosphate (MP Biomedicals, 157241), 10 ng/mL bFGF (Stemgent), 1 ng/mL TGF-β (StemRD, TGFB1-005), 10 ng/mL EGF (Stemgent), and 1× ITS (Insulin, Transferrin, and Selenium; VWR/Mediatech, 25-800CR) was added.

2.3.2 Virus coated culture plates

Sterile high binding 96-well plates (Greiner Bio-one) were coated with virus solutions at concentrations of 100 $\mu g \cdot mL^{-1}$ in 0.1 M potassium phosphate buffer (pH 7.0) or 20

ng·mL^{-1} hFN (BD, 354008) in PBS. Virus solutions were filtered before use by a 0.45 µm filter (PALL Life Sciences, Acrodisc Syringe Filter, 0.45 µm HT Tuffryn Membrane, Low Protein Binding, Non-pyrogenic, PN 4184, sterile). Plates were coated with filtered virus or hFN solutions for 20 min at room temperature and rinsed three times with water.

2.3.3 BMSC isolation and subculture

Primary BMSCs were isolated from the bone marrow of young adult 80 g male Sprague Dawley rats. The procedures were performed in accordance with the guidelines for animal experimentation by the Institutional Animal Care and Use Committee, University of South Carolina. Cells were maintained in serum media and split no more than four times after isolation before use in different experiments. BMSCs were split by removal of media, washed 2× with PBS, 1 ml Trypsin (0.25%), agitated lightly for 1-2 minutes until cells were detached, added 3 mL serum media, centrifuged at 700 *g* for 3 minutes, aspirated supernatant, re-suspend in media at appropriate concentration. For all experiments BMSCs were removed from cell culture plates as for a normal split. After adding 3 mL of serum media to deactivate trypsin, cells were centrifuged at 700 *g* for 2 minutes. The supernatant was removed; cells were washed with 3 mL of serum free media, and centrifuged at 700 g for 2 minutes. This wash was repeated 2 more times. During the final wash cells were counted and suspended in osteogenic serum free media at 70 cell·µL^{-1} then seeded into virus coated high binding plates at 100 µL·well^{-1}.

2.3.4 Cell spreading

Cell spreading was monitored via Calcien AM staining. At designated times cells were incubated with Calcein-AM (BD Bioscience) at 37 °C for 30 minutes. Cells were

then washed two times with PBS and measurements were taken using a fluorescence microscope (Olympus IX81 microscope using spinning disk) and fluorometer (MolecularDevices, SpectraMax M2e). The plate was read using an excitation wavelength at 490 nm and emission cutoff at 520 nm. Fluorescent images were analyzed using Slidebook 5.0 imaging software.

2.3.5 Alkaline phosphatase activity

Alkaline phosphatase activity was measured using p-nitrophenyl phosphate (Thermo, 37621). Cells were washed two times in PBS at ambient temperature. Cells were then fixed using 4% paraformaldehyde (Sigma-Aldrich, P6148) in PBS for 15 min at room temperature. Immediately after this cells were washed two times in PBS and 100 µL of PNPP solution was added to each well. The reaction was stopped after 15 or 30 minutes by adding 50 µL of 2 M sodium hydroxide to each well. The absorbance was measured at a wavelength of 405 nm on an ultraviolet-visible spectrophotometer (MolecularDevices, SpectraMax M2e).

2.3.6 Calcium quantification

Calcium build up was monitored via Alizarin Red (Sigma, A5533-25G,Cas: 130-22-3) staining. Cells were washed two times in PBS at ambient temperature and then fixed using 4% paraformaldehyde (Sigma-Aldrich, P6148) in PBS for 15 min at room temperature. Immediately after this cells were washed two times in water and covered with 0.1% Alizarin Red (pH 4.2), overnight at 4 °C. Cells were then washed two times with water at ambient temperature and images were taken or 100 µL of 0.1 M sodium hydroxide was added to each well. The absorbance was measured at a wavelength of 548

nm on an ultraviolet-visible spectrophotometer (MolecularDevices, SpectraMax M2e). Images were taken on a microscope (Olympus IX81 microscope).

2.3.7 ELISA

Cells were fixed in 4% paraformaldehyde (Sigma-Aldrich, P6148) in PBS for 15 minutes at room temperature. The cells were washed and blocked with 1% BSA/1x D-PBS/0.05% Triton X-100 for 1 hour. The primary antibodies against osteopontin and osteoclacin were incubated in wells overnight at 4 °C at a dilution of 1:100. The samples were rinsed with PBS, 0.05% Triton X-100, three times and the secondary antibody (anti-mouse Goat polyclonal with HRP conjugate) was incubated for 1 hour at room temperature. The samples were washed three times and incubated with 3,3',5,5'-tetramethylbenzidine solution for 30 minutes and the reaction was stopped with concentrated sulfuric acid. The solution absorbance was read with an ultraviolet-visible spectrophotometer at 450 nm.

2.3.8 Virus Purification.

Native TMV and its mutant variants were purified according to previously reported method [14]. The infected leaves were collected and stored in Ziploc bags (~100−150 g of leaves per bag) and stored in −80 °C freezer for later processing. For purification, the frozen leaves were crushed by hand and then transferred to a 1.5 L blender (Oster). Approximately 3 volumes of phosphate buffer were added to the crushed leaves with an addition of 0.2−0.3% 2-mercaptoethanol. The leaves were blended for 2 min at low setting and then switched to highest setting for an additional 3 min. The blended plant sap was filtered through two layers of cheesecloth and then flow through was centrifuged at

13500 rpm (Sorvall SLA1500) at 4 °C for 30 min. The resulting supernatant was then pooled together and mixed with n-butanol/chloroform at a ratio of 2:1:1 (plant sap/n-butanol/chloroform). The homogenate was stirred for 30 min on ice and then centrifuged at 12500 rpm (SLA 1500) for 20 min at 4 °C. The aqueous layer was transferred to a beaker, and the virus was precipitated by adding 0.2 M NaCl and 8% (wt/vol) PEG-8000. The mixture was stirred on ice for 60 min and centrifuged at 13500rpm (Sorvall SLA1500) for 20 min. The white precipitant was then resuspended with 10 mM K phos buffer (pH 7) supplemented with PMSF protease inhibitor (10 μg/mL final concentration). The solution was centrifuged at 9,500 rpm for 10 min at 4 °C to remove excess PEG. The supernatant was transferred to ultracentrifuge tubes (Beckman 50.2 Ti) and the virus was pelleted at 42,000 rpm at 4 °C for 2.5 h. The virus pellet was resuspended in 100 mM K phos buffer (pH 7) overnight at 4 °C. The virus solution was centrifuged again at 9500 rpm for 10 min at 4 °C to remove insoluble debris. UV absorbance was measured at 260 and 280 nm to determine the concentration of the virus. The virus concentration of 0.1 mg/mL has an absorbance of 0.3 at 260 nm and exhibits a characteristic 260/280 ratio of 1.26−1.27. The purified virus solutions were aliquoted and stored at −20 °C freezer.

2.3.9 Atomic Force Microscopy

Tapping-mode atomic force microscope (AFM) images were obtained at ambient conditions using Nanoscope IIIA Multi Mode AFM (Veeco). Si tips with a resonance frequency of approximately 300 kHz, a spring constant of about 40 N m^{-1}, and a scan rate of 0.75 Hz were used.

2.4 RESULTS

2.4.1 Experimental design

Two sets of experiments have been performed. The first set of experiments used genetically mutated viruses or native TMV as substrates to support the differentiation of MSCs (Figure 2.1 a). The second set of experiments determined effect of virus shape on differentiation of MSCs (Figure 2.1 b). For the first set of experiments virus particles were coated onto substrates (for experimental details see section 2.4.2). Then cells were seeded on these substrates and induced with osteogenic media. The cells were then monitored while undergoing osteogenic differentiation. For the second set of experiments a virus mutant was either left whole or broken into its individual coat protein subunits and then coated onto substrates (Figure 2.1 b). MCS were then seeded (in serum free conditions) onto the substrates and induced with serum free osteogenic media. MSCs were then monitored over a 21 day period for expression of various osteogenic markers.

2.4.2 Virus coated culture plates

Stable virus and virus mutant substrates were made by coating high protein binding plates with the various virus types. High binding plates were either coated with virus particles or virus subunits (Figure 2.1 a, b). After coating, substrates were washed to remove excess virus or virus subunits and allowed to dry.

Virus mutants were previously made by genetically fusing a cell binding motif to the surface-exposed, carboxy end of the coat protein [14]. The native and mutant viruses display 2130 identical copies of coat protein per virus particle. This leads to the cell binding motifs being displayed in a highly uniform manner. Inserts are separated from each other by ~ 3 nm, as defined by the structural organization of viral capsid [14].

a

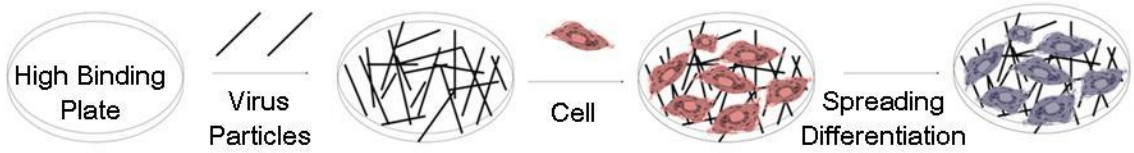

b

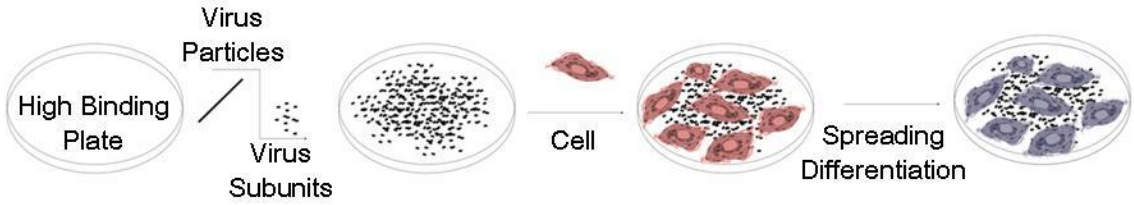

c

Virus	Insert	Location	MALDI	Protein
TMV			17534	
RGD1	GRDSPG	155	18161	Fibronectin
DGEA	DGEA	155	17908	Collagen
PHSRN3	EDVRPHSRNSIT	155	18927	Fibronectin
P15	GTPGPQGIAGQRGVV	155	18910	Collagen

Figure 2.1 Schematic illustration of fabrication process for virus mutant substrates with AFM and contact angle analysis of virus mutant substrates. a) High protein binding plates were covered with virus or virus subunit solutions. Then excess solution was washed off. MSCs were seeded on virus mutant surfaces and monitored over 21 days for spreading and differentiation. b) Stability of virus mutant substrates was monitored over 24 hours in cell media. Coating of various virus mutants on high binding plates was analyzed by AFM and contact angle. c) Table of virus mutants used. Column one is the names of each mutant used. Columns two and three are the specific peptide sequences and inserted into each virus mutant and their insert locations. Column four is the MALDI determined mass of the virus mutant coat protein subunits. Column five is the specific matrix proteins that the inserts were derived from

The mutants used in these experiments along with their inserted motifs are listed in Figure 2.1 (c).

Several different concentrations of virus solution were tested for their ability to deposit virus on the high binding substrates. It was found that 100 $\mu g \cdot mL^{-1}$ deposited viral particles on the substrate effectively (Figure 2.2 b). This concentration for coating was used for all cell studies. A similar experiment was done with virus coat protein subunits. Various concentrations of coat protein subunit solutions were tested for their ability to deposit virus coat protein on the high binding substrates. It was found that a 10 $\mu g \cdot mL^{-1}$ solution of virus coat protein could deposit a similar amount of virus coat protein as the 100 $\mu g \cdot mL^{-1}$ virus solution. This concentration was used for all cell studies.

To visually inspect the coverage of virus particles on the virus substrates, AFM micrographs were taken. The micrographs in Figure 2.2 (c) show the coverage after using 100 $\mu g \cdot mL^{-1}$ solution of virus particles on high protein binding surfaces. To monitor the stability of the coating and determine change in surface coverage, virus coated substrates were soaked in serum free media for 24 or 48 hours at 37 ^{o}C (typical cell culture conditions). No significant change in virus coating was observed after this time (Figure 2.2 c).

Virus deposition onto the high binding surface was further analyzed by contact angle. Contact angle measurements were taken of the substrates before and after the various virus types had been deposited. It is well known that the contact angle of a surface depends on surface composition. It was found that the underlying substrate before deposition had a contact angle of 89.0 ± 2.3^{o}. After coating the high protein binding surfaces with either native TMV or RGD1 mutant the contact angle changed to 77.6 ± 4.6

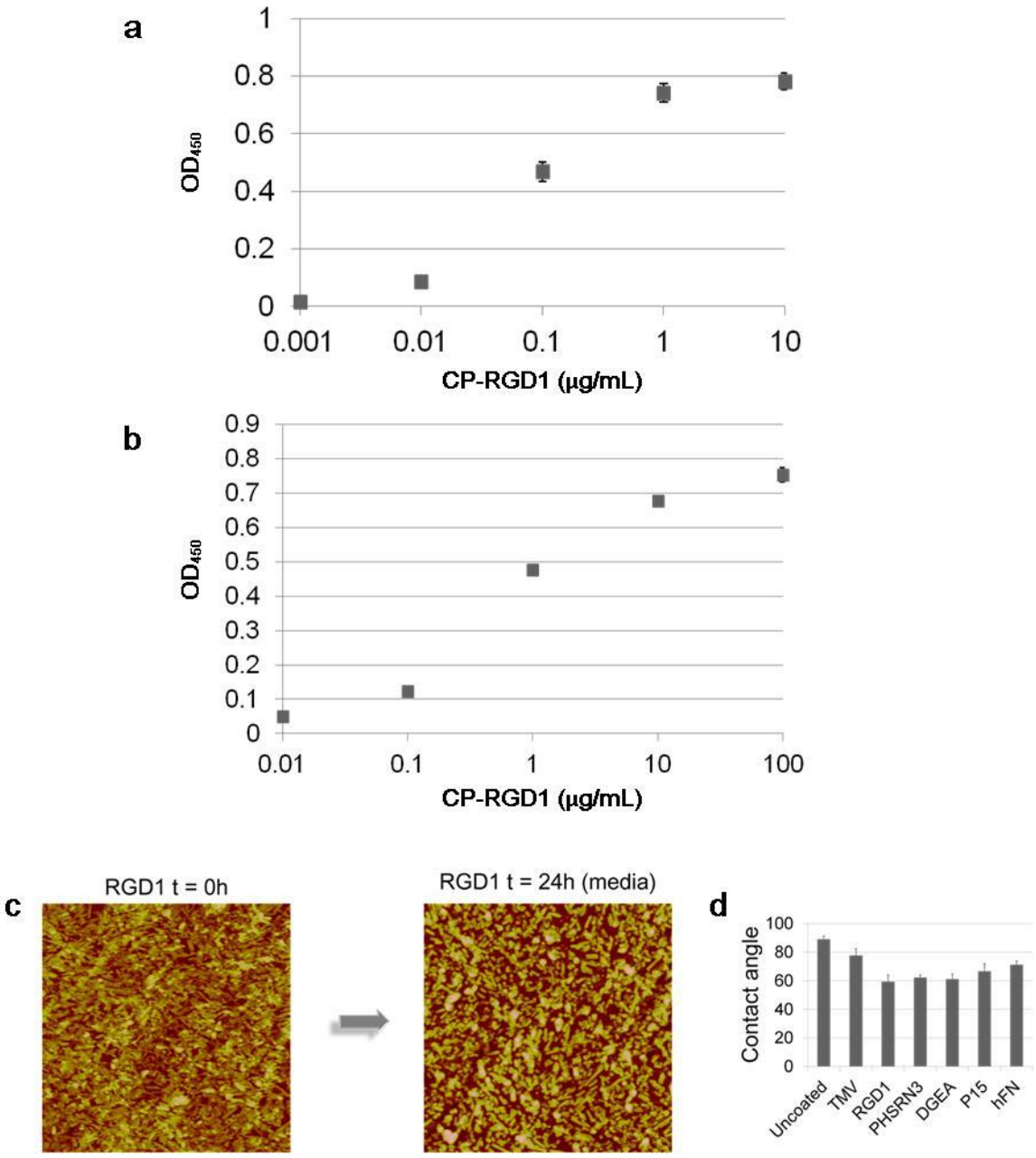

Figure 2.2 Optimization of virus coat protein and virus particle deposition on high binding plates. a) and b) Deposition of coat protein or virus particles from different concentrations of coat protein or virus particles. Deposition was measured using ELISA. c) Stability of virus substrates. AFM images of virus substrate after 24 hours in cell media. d) Contact angle of high binding plates before and after virus deposition.

or 59.0 ± 4.5^{o} respectively. The rest of the mutants had contact angles between these two extremes. It should be noted that a pure TMV film has a contact angle around 45.5 ± 2.7^{o} and the contact angle of pure RGD1 film has not been determined. We assume that it would be similar to that of native TMV (or slightly lower due to the added charged residues) because of their high degree of structural and compositional similarity. The contact angles of the virus coated surfaces were between that of a pure TMV surface and the uncoated surface. This showed virus was being deposited on the surface. The homogeneity of the coating can be seen in the representative micrographs in Figure 2.2 (c).

2.4.3 Cell spreading on individual mutants

Cell spreading and morphology were monitored for two reasons. First morphology and spreading are good indicators of surface biological inertness or toxicity. Second cell morphology can be an early indicator of changes in cell processes such as differentiation. MSCs going through osteogenic differentiation change to a polygonal morphology. Furthermore, production of a self mineralized matrix marks the terminal stages of osteogenic differentiation.

Initial cell attachment was observed by bright field microscopy at 24 hours. At this time cells had attached and begun to spread on all surfaces. However, there was no observable difference (by eye) between the surface types.

For quantitative cell spreading studies, MSCs were seeded on virus coated substrates and kept under serum free conditions in osteogenic media and observed at 7, 14, and 21 days. Spreading was observed in two ways: fluorescent microscopy and by fluorometer (Figure 2.3). Fluorescent images were analyzed using Slidbook5. Cell coverage was

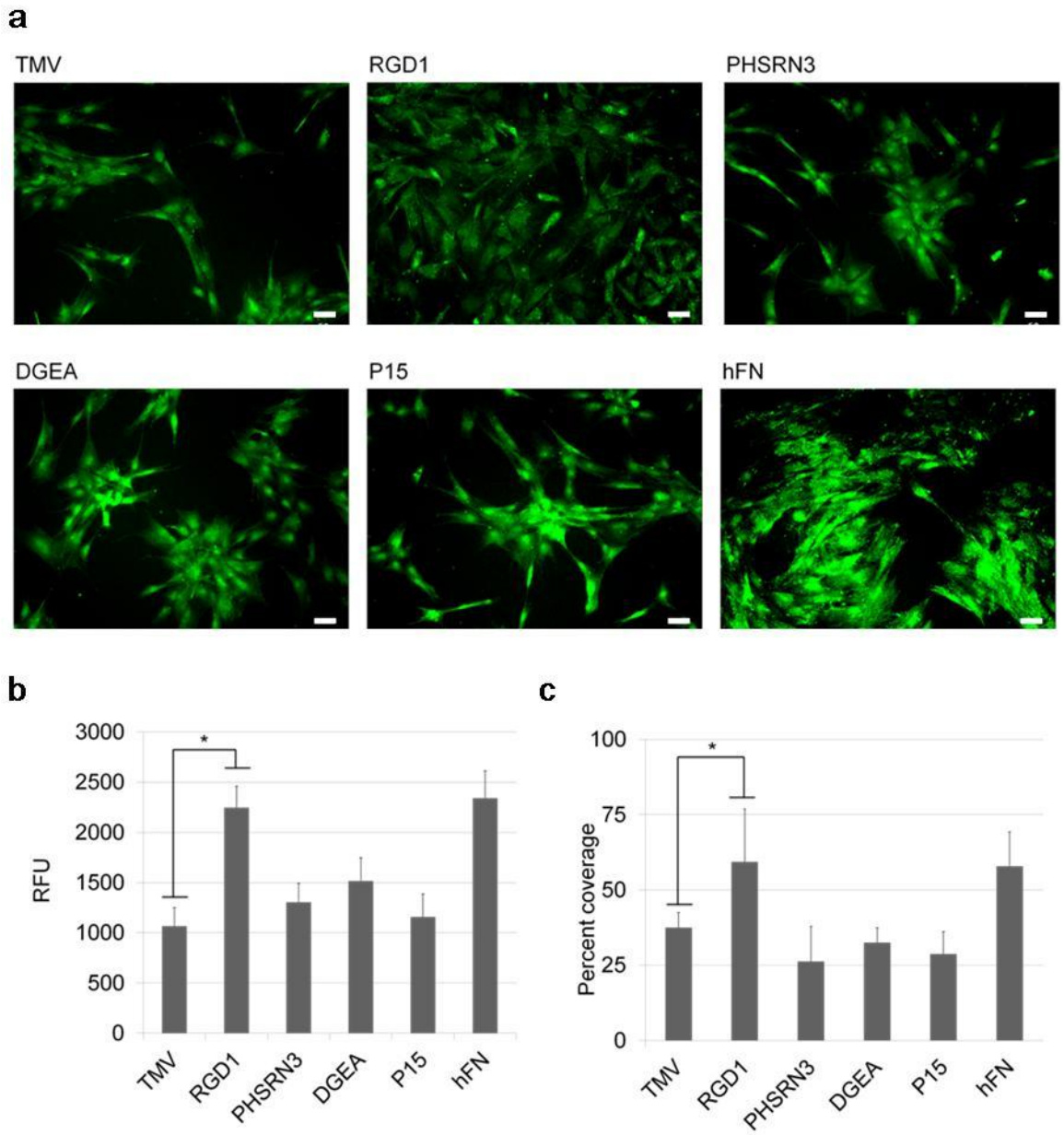

Figure 2.3 Cell spreading on virus substrates. a) Fluorescent microscopy images of MSCs on mutant substrates. Quantification of MSC spreading by b) fluorometer and c) image analysis. Cells were stained with Calcein-AM. Results shown here are for day 14. MSC cell spreading was measured at days 7, 14 and 21. Bars correspond to mean ± standard deviation, (*) $p < 0.05$ obtained from paired student's t-test. No significant difference, for each sample, was observed between time points. Scale bars are 50 μm.

determined by the ratio of green pixels to total pixels for each image. The average was determined from ten images of each sample type. For the fluorescence measurements, the average for each sample type was taken from three wells (Figure 2.3 c). Notice that the trend and relative differences between samples are similar for either method of analysis. Because of this observation and ease of use, fluorescence measurements were used for the rest of the cell spreading experiments.

MSCs on native TMV and the rest of the virus mutant substrates showed less spreading. Even with this decreased spreading the cells were healthy. This was proven by the spreading measurements done at day 14 and 21. At these two time points there was not a significant change in the cell spreading from the initial day 7 measurement. The spreading measurement for day 14 is shown in Figure 2.3.

2.4.4 Alkaline phosphatase activity on individual mutants

Alkaline phosphatase activity is commonly used as a differentiation marker. Alkaline phosphatase is a known phosphatase enzyme that is expressed in cells differentiating into osteoblasts. The three separate periods defined for osteogenic differentiation are: 1) proliferation and production of ECM; 2) ECM development and maturation; and 3) mineralization [69]. The activity of alkaline phosphatase rises as the cells proliferate and reaches a maximum as cells mineralize. After mineralization the alkaline phosphatase activity drops off. Alkaline phosphatase activity was measured through a p-nitrophenyl phosphate (PNPP) assay. The PNPP substrate is cleaved by phosphatases including alkaline phosphatase. The reaction yields p-nitrophenol (yellow) which is then detected with an ultraviolet-visible spectrophotometer. As can be seen in Figure 2.4 alkaline phosphatase activity in MSCs has peaked by day 14 on both the RGD1 mutant and hFN

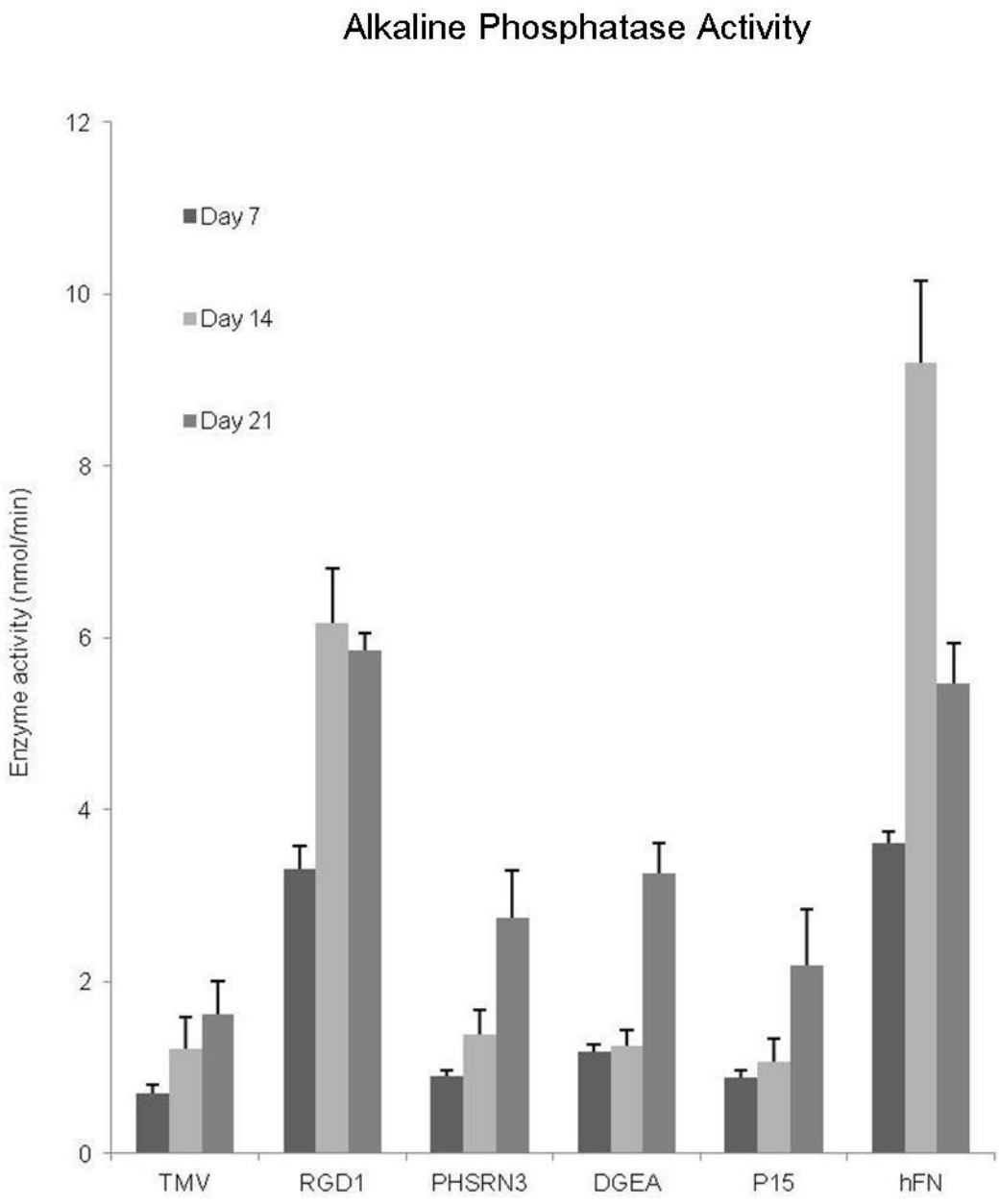

Figure 2.4 Alkaline phosphatase activity on whole virus mutant substrates. Alkaline phosphatase activity is increased in cells on RGD1 and hFN substrates by day 7. Cells on native TMV and the rest of the virus mutants show no significant increase in activity until day 21. Bars correspond to mean ± standard deviation, n = 3.

substrates. It is impossible to say when exactly alkaline phosphatase activity peaked in MSCs on these two samples because of the intermittent sampling. What can be concluded is that alkaline phosphatase activity had dropped off by day 21 and the cells on these two substrates had already entered into mineralization, the final stage of osteogenic differentiation. Furthermore, MSCs on the native TMV and other mutant coatings had alkaline phosphatase activity that was still increasing by day 21. This showed that cells on these substrates were still in one of the first two stages of osteogenic differentiation.

2.4.5 Calcium quantification on individual mutants

Calcium deposition was observed with alizarin red staining at days 7, 14, and 21. After cells were stained they were imaged and a pink color was observed in all samples (Figure 2.5). However, there was no discernible difference (by eye) between samples. To quantify the calcium accumulation we used a modified method from literature [70]. This method uses alizarin red staining and ultraviolet-visible spectrophotometry. This was done at days 7, 14, and 21. Each sample had an n=3. On day 7 calcium deposition in the RGD1 and hFN samples was nearly double that of the other samples (TMV, PHSRN3, DGEA and P15). At day 14 the calcium deposition was further increased in the RGD1 and hFN samples but had not increased in any of the other samples. At day 21, calcium deposition continued to rise in the RGD1 and hFN samples. Also at this time an increase was seen in the TMV, PHSRN3, DGEA and P15 samples.

2.4.6 Osteopontin and osteocalcin expression on individual mutants

Osteopontin and osteocalcin are noncollagenous proteins that are expressed in a specific manner during the three periods of osteogenic differentiation. The three separate

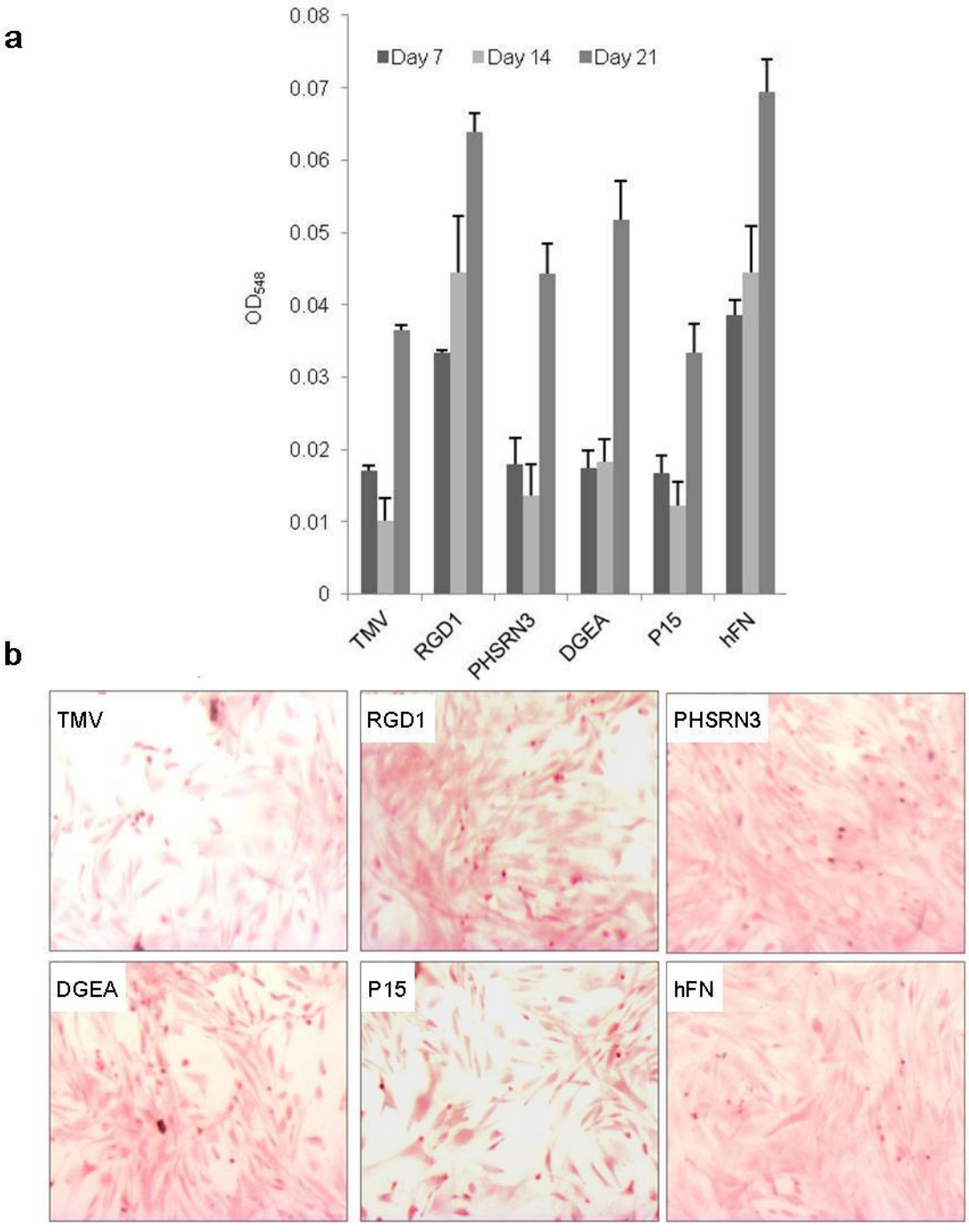

Figure 2.5 Calcium deposition in MSCs. a) Calcium quantification by alizarin red staining of MSCs on virus substrates. b) Images of MSCs after alizarin red staining at day 14. Calcium deposition is increased in MSCs on RGD1 and hFN control as early as day 7 as compared to native TMV and the other virus mutants. Bars correspond to mean ± standard deviation, n = 3.

periods defined for osteogenic differentiation are: 1) proliferation and production of ECM; 2) ECM development and maturation; and 3) mineralization [69].

Osteopontin is one of the earliest markers of osteogenic differentiation and is expressed in the proliferation period. After this its expression decreases during the second period of ECM development before increasing again during the final mineralization period. Osteopontin quantification was chosen for this study because it specifically localizes to cell-matrix and matrix-matrix interfaces and can bind to various extracellular molecules including collagen and fibronectin [71]. Our results show that at day 14 (Figure 2.6) osteopontin expression in MSCs grown on fibronectin (hFN) was lower than MSCs grown on all the other substrates including RGD1. This indicates that MSCs on hFN had finished proliferation and were somewhere in the ECM maturation period of osteogenic differentiation. This result coupled with the calcium deposition result (Figure 2.5) suggests that MSCs on this substrate were finishing EMC maturation and entering mineralization at day 14. As mentioned the osteopontin expression in all other substrates was increased at day 14. This data taken alone means that MSCs on these substrates were either in the first proliferative period or in the final mineralization period of osteogenic differentiation at day 14. When taken with the calcium deposition data for day 14 (Figure 2.5), this data suggests that MSCs on TMV, DGEA, PHSRN, and P15 substrates were all in the proliferation period of osteogenisis and that MSCs on RGD1 substrates were in the final mineralization period at day 14.

Osteocalcin is a bone tissue-specific gene that binds calcium and accumulates in the extracellular matrix. It is believed to play a critical role in the mineral phase formation in

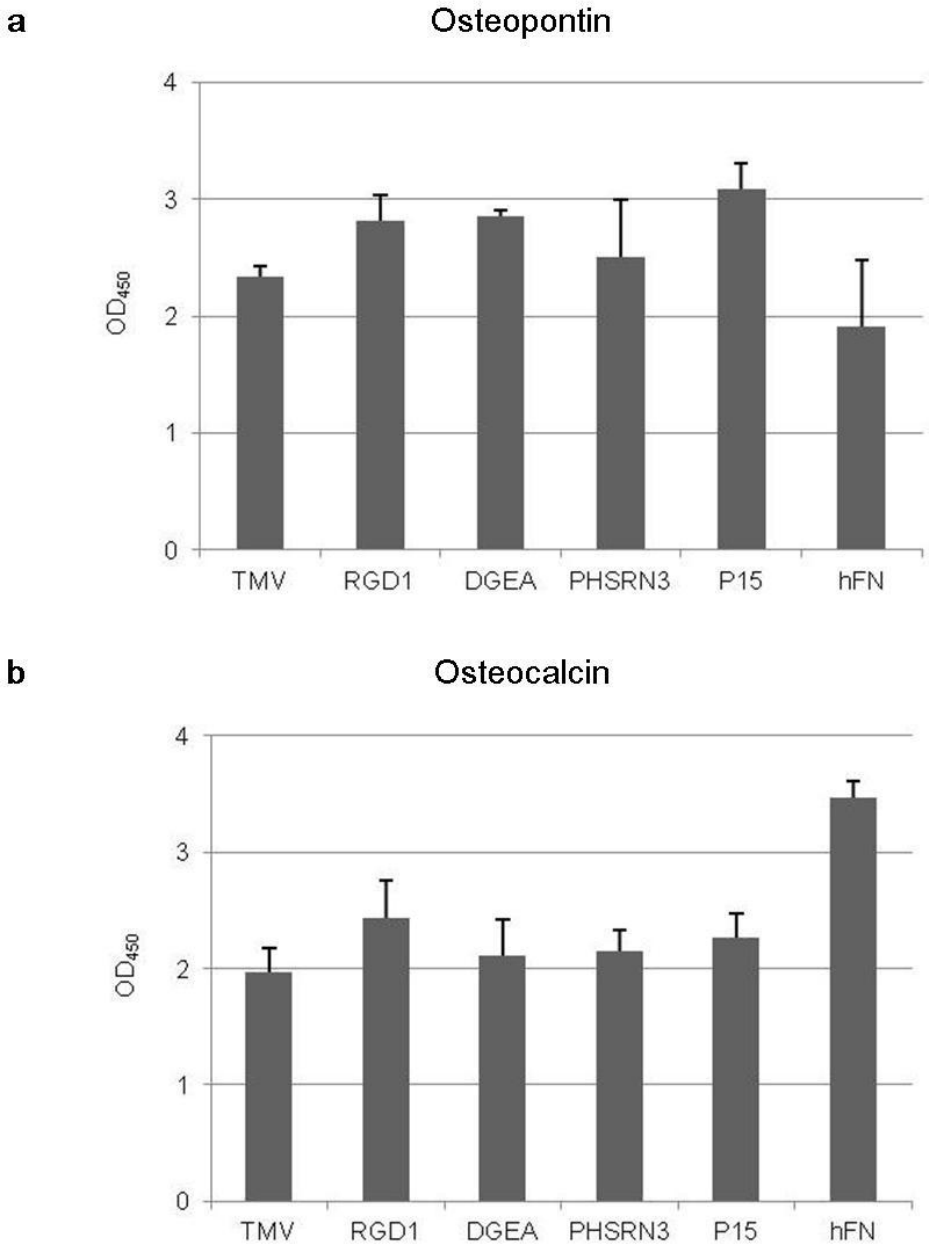

Figure 2.6 a) Osteopontin and b) osteocalcin expression by MSCs (quantification by ELISA) on whole virus substrates. Osteopontin and osteocalcin expression was measured in MSCs at day 14. Bars correspond to mean ± standard deviation, n = 3.

bone [72]. Osteocalcin is expressed during the ECM maturation period and reaches a maximum during the mineralization period [73]. After this peak its expression drops off.

Our data shows that at day 14 MSCs grown on hFN had a significant increase in osteocalcin levels compared to MSCs grown on other substrates (Figure 2.6). This data further corroborates what was seen with the calcium deposition and osteopontin data. It suggests that at day 14 MSCs on hFN substrates were transitioning from the ECM maturation period into the final mineralization period. Furthermore, osteocalcin expression of MSCs on all other substrates at this time point was significantly lower than MSCs on hFN. This means that MSCs on these substrates were either in pre- or post-mineralization period. To confirm which we look at the calcium deposition data for these substrates and can see that it is likely that at day 14 MSCs on RGD1 substrates are in the final mineralization period of osteogenesis and MSCs on all other virus substrates are still in the proliferative period of osteogenesis.

2.4.7 Cell spreading on coat protein subunits

The first set of experiments showed that the RGD1 mutant supported substrates can shorten the time to onset of mineralization of MSCs. It is possible that either the ordered arrangement of the binding motifs on the virus or the roughness created by the virus particles are responsible for this observation. To test this, RGD1 virus particles were broken into their individual coat protein subunits and coated onto high binding substrates.

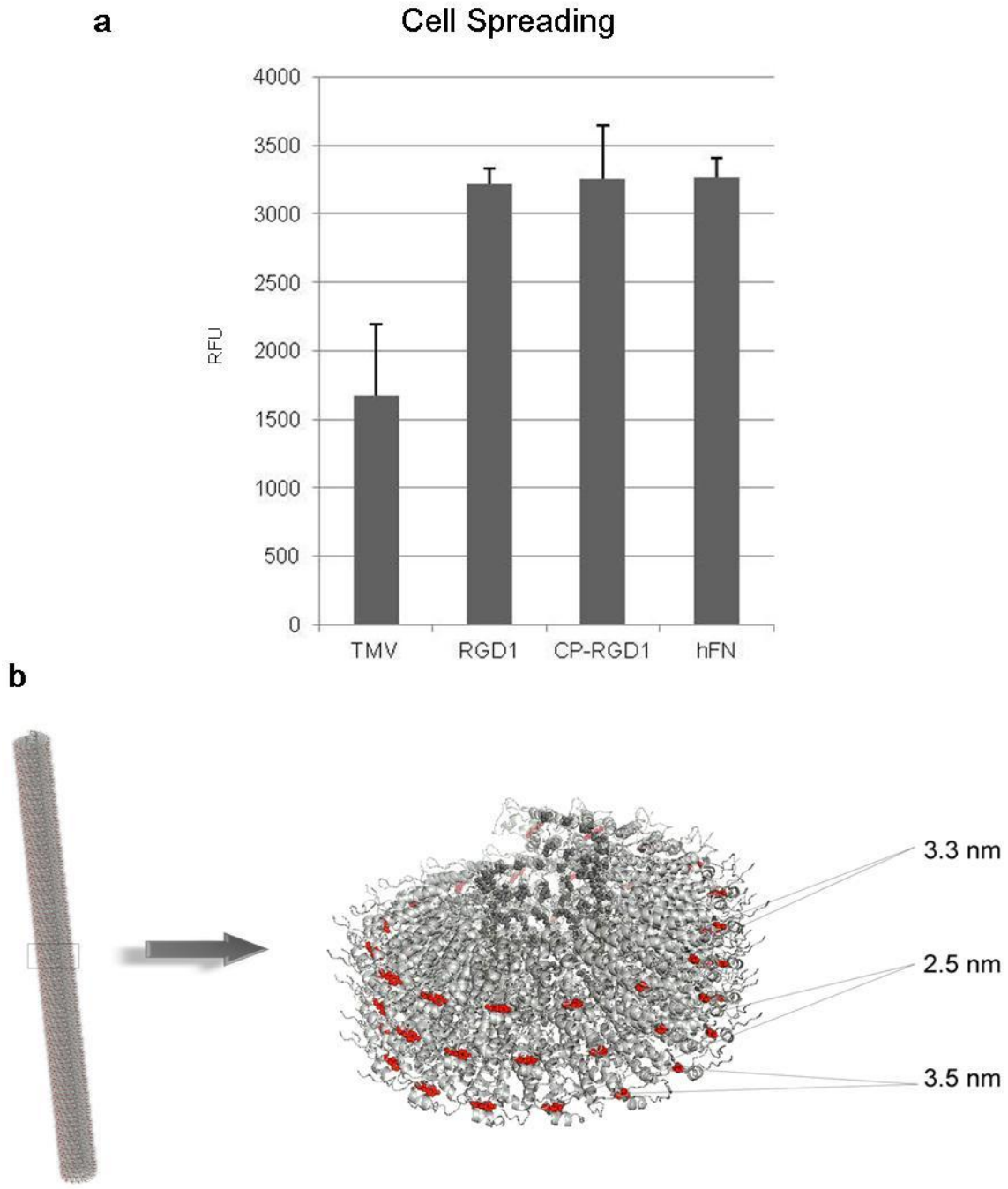

Figure 2.7 Cell spreading on RGD1 coat protein substrates. (a) MSC spreading on CP-RGD1 substrates is not significantly different from RGD1 and hFN substrates. (b) Pymol illustration showing ordered arrangement of binding motifs that is disrupted when CP-RGD substrates are made.

Cell spreading studies on coat protein subunits were done as earlier experiments. MSCs were seeded on virus and coat protein coated substrates and kept under serum free conditions in osteogenic media. Attachment and spreading was observed at day 14. Spreading was observed via fluorometer. For the fluorescence measurements the average for each sample type was taken from three wells. Initial cell attachment was observed by bright field microscopy at 24 hours. At this time cells had attached and begun to spread on all surfaces. However, there was no observable difference (by eye) between the surface types. Cell spreading was quantitatively measured at day 14 (Figure 2.7 a). Cell spreading was not significantly different on RGD1 (RGD1 mutant), CP-RGD1 (RGD1 coat protein subunits), or on the hFN control. As seen in earlier experiments MSCs on the native TMV surface showed the least amount of spreading. Even with this decreased spreading the cells were healthy. These results suggest that the RGD insertion is the major factor attributing to cell attachment and spreading.

2.4.8 Alkaline phosphatase activity and calcium quantification on coat protein subunits

As mentioned earlier alkaline phosphatase is a known phosphatase enzyme that is expressed in cells differentiating into osteoblasts. Its activity rises as the cells proliferate and reaches a maximum as cells mineralize. After mineralization alkaline phosphatase activity drops off. Alkaline phosphatase activity of MSCs on CP-RGD1 substrates was measured at days 7 and 14. It was found that alkaline phosphatase activity at day 7 or day 14 in MSCs on CP-RGD1 substrate was not significantly different from RGD1 or hFN substrates (Figure 2.8). These results indicate that neither the ordered spacing of the binding motifs nor the virus shape play a significant role in the activity of alkaline

phosphatase. And as seen in original experiments MSCs on RGD1 and hFN substrates have significantly higher alkaline phosphatase activity than MSCs on TMV substrates for both days 7 and 14 (Figure 2.8). MSCs on CP-RGD1 substrates had their calcium quantified by alizarin red staining at days 7 and 14. It was found that calcium deposition of MSCs on the RGD1, CP-RGD1 and hFN was not significantly different (Figure 2.8). These results indicate that neither the ordered spacing of the binding motifs nor the virus shape play a significant role in calcium deposition. However as seen previously the calcium deposition of MSCs on RGD1 and hFN is nearly double that of the TMV samples.

2.4.9 Osteopontin and osteocalcin expression on coat protein subunits

As previously mentioned osteopontin and osteocalcin are noncollagenous proteins that are expressed in a specific manner during the three periods of osteogenic differentiation. Osteopontin is one of the earliest markers of osteogenic differentiation and is expressed in the proliferation period. Then its expression decreases during the second period of ECM development before increasing again during the final mineralization period. Osteopontin expression of MSCs on CP-RGD1 substrates was quantified at day 14. It was found that osteopontin expression of MSCs on CP-RGD1 substrates was significantly lower than MSCs grown on RGD1 substrates. However it was not as low as MSCs grown on hFN substrates (Figure 2.9). This indicates that MSCs on hFN and CP-RGD1 substrates had finished proliferation and were somewhere in the

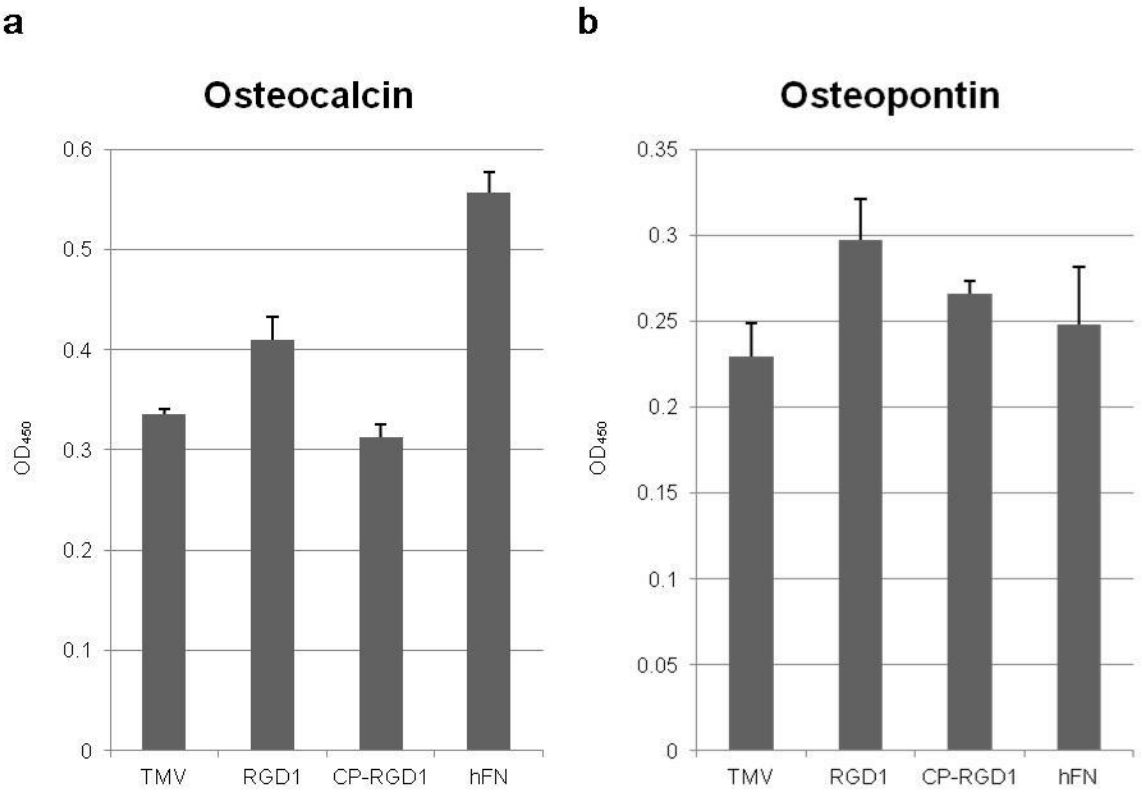

Figure 2.9 a) Osteopontin and b) osteocalcin expression by MSCs (quantification by ELISA) on RGD1 coat protein substrates. Osteopontin and osteocalcin expression was measured in MSCs at day 14.

ECM maturation period of osteogenic differentiation. This result coupled with the calcium depositon results (Figure 2.8) suggests that MSCs on these two substrates were finishing EMC maturation and entering mineralization at day 14. While MSCs on RGD1 substrates were in the middle of mineralization. These results indicate that either the ordered spacing of the binding motifs or the virus shape affect rate of differentiation.

Osteocalcin is expressed during the ECM maturation period and reaches a maximum during the mineralization period. After this peak its expression drops off. Osteocalcin expression of MSCs on CP-RGD1 substrates was quantified at day 14. It was found that osteocalcin expression of MSCs on CP-RGD1 substrates was significantly lower than osteocalcin expression of MSCs on RGD1 or hFN substrates (Figure 2.9). This indicates that MSCs on CP-RGD1 substrates were in an earlier stage of differentiation than those on RGD1 or hFN substrates. This corroborates the osteopontin results.

2.5 CONCLUSION

This study used genetically mutated viruses as substrates to support and improve the differentiation of mesenchymal stem cells into osteoblasts. Substrates were made by coating high protein binding plates with either virus mutant particles or individual mutant coat protein subunits. AFM images, contact angle measurements, and ELISA quantification showed that virus particles and coat protein subunits were deposited on the substrate surfaces. ELISA quantification showed deposition was concentration dependent for both virus particles and coat protein subunits. When virus substrates were used for cell culture, it was found that virus substrates did support the differentiation of MSCs. Furthermore, substrates made from RGD1 virus mutants decreased the time to onset of

mineralization. Additionally it was showed that the ordered spacing of the binding motifs or the virus shape played a significant role in the rate of differentiation of MSCs into osteoblasts.

CHAPTER 3

VIRUS MUTANT BASED SCAFFOLDS FOR THE ALIGNMENT AND DIFFERENTIATION OF NEUROBLAST AND MYOBLAST CELLS

3.1 ABSTRACT

This study used RGD ligand displaying rod-shaped virus particles to create ordered substrates that were then used for the alignment and differentiation of neuroblast and myoblast cells. Viruses were aligned on the concave surface of glass capillary tubes with a flow based assembly method. To achieve the alignment, a polypropylene feeder tube was filled with virus solution and connected to a glass capillary tube, and then the virus solution was forced through the glass capillary using high pressure N_2. Finally the glass capillary was dried using high pressure N_2. Virus alignment and coverage was controlled by the flow rate, surface properties, and virus concentration. This type of alignment was different from our previous work (see Chapter 1) because rod-shaped viruses were arranged parallel to the long axis of the capillary tube. Myoblasts and neuroblasts were grown on aligned and unaligned virus substrates. It was found that myoblast actin filaments aligned with the underlying virus substrates. In addition, while neuroblast neurite extensions did not align with the underlying virus substrates, the length of neuroblast neurite was significantly increased on aligned virus substrates.

3.2 INTRODUCTION

Material formation

Anistropic nanoparticles have become increasingly used in modern materials with nanoscale features. Furthermore, the alignment of these nanoparticles is crucial to final material properties [74, 75]. For example, it has been shown that both electrical and thermal conductivity of carbon nanotubes increases along the direction of alignment; and enhancement was strongly dependent on degree of alignment [76, 77]. As alignment is important there are a variety of methods to direct nanorod orientation including contact shear force, [78-80] electric field, [81] fluid flow, [82-84] surface pressure [85], surface chemical functionalities, [86] micropatterns fabricated by lithography [87] or capillary force at a contact line during a drying process [88]. The ability to control nanorod and nanotube orientation gives rise to functional and valuable materials for wide applications in tissue engineering, [89] medicine, [90] electronics, [82] and optical devices [91]. In this chapter we use a general, rapid and simple method for aligning rod-shaped viruses that can be used on a larger scale and applied to different types of nanorods.

Myoblasts and neuroblasts

Myoblasts and neuroblasts were chosen for these studies because it is important to understand what affects alignment and differentiation in these two cell types. Alignment and differentiation of myoblasts is key to creating therapies for skeletal and heart muscle defects [92, 93]. Alignment and differentiation of neuroblasts is key to creating therapies for treating spinal and peripheral nerve damage [94].

To create functional replacements for damaged muscle tissue (cardiac and skeletal) it is essential that the replacements contain aligned replacement cells [97, 98]. Alignment is important because it correlates to contractile strength, rapid electrical propagation and the alignment of sarcomeres. Which in turn contribute to spatially and temporally ordered contraction [92, 95]. In addition, differentiation of myoblasts into myocites (myogenesis) is important for cell based therapies to treat heart disease or skeletal muscle defects. These therapies require functional replacements for damaged cells. Often the best source of functional cells is stem cells that have first been differentiated into myoblasts. The work presented here differs from conventional studies that consider the effects of soluble factors [99, 100] and concentrates on the use of materials for the alignmnent and differentiation of myoblasts.

Control over neurite outgrowth is important in creating therapies for treating spinal and peripheral nerve damage. Most therapies use conduits to control neurite outgrowth [101, 102]. These conduits' primary functions are to contain nerve growth and give physical support for neurite outgrowth. However recent approaches have expanded by using other cell sources such as stem cells [103, 104]. When stem cells are used cells must be differentiated aligned to create functional replacements. Therefore understanding cell differentiation into neurons is important for creating cell based therapies for treating spinal and peripheral nerve damage.

3.3 MATERIALS AND METHODS

3.3.1 Media

Serum free media, DMEM high glucose, was made by adding 6.7 g powder media (Hyclone, SH30003.03), 1.2 g sodium bicarbonate (Fisher Scientific , S233-500), 3.57 g HEPES (Cellgro, 61-034-RM), 5.0 mL L-glutamine solution (Invitrogen, 25030081), and 5 mL penicillin-streptomycin (Invitrogen, 15140122) to 500 mL water (Millipore Synergy UV system, 18.2 MΩ.cm). The solution was then brought to pH 7.4 using 1 M sodium hydroxide solution (J.T. Baker, E31H10). The media was sterilized by vacuum filtration using a low protein binding media filter (Corning 0.22 μm, 431097).

Serum media was prepared as serum free media with the addition of 50 mL fetal bovine serum (FBS) after filtration (Atlanta Biologicals, S12450).

3.3.2 Virus alignment in capillary tubes

Borosilicate glass capillary tubes (inner diameter 0.15 cm, KIMBLE Co.) were cleaned and sterilized with a piranha solution (7:3 mixture of 98% H_2SO_4 and 30% H_2O_2) at 75 ^oC for 2 hours. These were stored under water or ethanol until use. All following steps used filter sterilized solutions and aseptic technique. Directly before patterning tubes were rinsed with water and dried thoroughly with N_2 gas. Tubes were then submerged in one of 3 polymer solutions: Chitosan, PDDA (poly), or PLL (poly) for 1 hour. Tubes were then rinsed with water and dried with N_2 gas. Tubes then had a solution of virus (TMV or RGD1) blown through at 4 psi using a N_2 stream. Nitrogen continued to be blown through the tubes until they were dry. The tubes were then cut to 2 cm lengths, externally wiped with ethanol, and used in cell culture experiments.

3.3.3 N2A cell culture

N2A cells were maintained in serum media, split 1:10 twice a week, and media was changed every 48 hours. N2A cells were split by: removing serum media, washing two times with D-PBS, releasing the cells with 1 mL trypsin (Invitrogen, 2500056), adding 9 mL serum media, separating into new flasks containing 9 mL serum media.

3.3.4 C2C12 cell culture

C2C12 cells were maintained in serum media, split 1:6 every 4 days, and media was changed every 48 hours. C2C12 cells were split by: removing serum media, washing two times with D-PBS, releasing the cells with 1 mL trypsin (Invitrogen, 2500056), adding 3 mL serum media, separating into new flasks containing 9 mL serum media.

3.3.5 C2C12 culture in virus aligned tubes

C2C12 cells were removed from cell culture plates as for a normal split. After adding 3 mL of serum media to deactivate trypsin, cells were counted and centrifuged at 700 g for 3 minutes. The supernatant was removed and cells were suspended in serum media. This cell solution was injected into capillary tubes using a micropipette. The tubes were placed in the bottom of a 12 well cell culture dish and placed in an incubator overnight. After cells had attached to the luminal surface of the tubes, tubes were moved to cell culture wells containing 1 mL of serum media. Media was changed in wells every 48 hours.

3.3.6 N2A culture in virus aligned tubes

N2A cells were removed from cell culture plates as for a normal split. After adding 9 mL of serum media to deactivate trypsin, cells were counted and centrifuged at 700 g for

2 minutes. The supernatant was removed, and cells were washed with 3 mL of serum free media, and centrifuged at 700 g for 2 minutes. This wash was repeated 2 more times. During the final wash cells were counted and suspended in serum free media. This cell solution was injected into the virus coated capillary tubes using a micropipette. The tubes were placed in the bottom of a 12 well cell culture dish and placed in an incubator overnight. After cells had attached to the luminal surface of the tubes, tubes were moved to cell culture wells containing 1 mL of serum media.

3.3.7 Cell staining and imaging

C2C12 cells were grown in virus coated tubes for 7 days. Tubes were then gently washed two times with PBS, fixed with 4% paraformaldehyde (Sigma-Aldrich, P6148) in PBS for 15 minutes, and then washed again twice with PBS. Cells were then blocked for 90 minutes by a solution of 0.5% TritonX100 and 1% BSA. Actin filaments and nuclei were stained for 1 hour using a solution of 1:500 rhodamine-phallodin and 1:5,000 DAPI. Cells were then washed 4× using PBS. The final wash was left overnight, at 4^{o} C, and light protected. N2A cells were grown on virus coted tubes for 48 hours and then imaged live. Differential interference contrast and fluorescence images were taken using an Olympus IX81 microscope using spinning disk.

3.3.8 ImageJ analysis

Neurite and actin filament alignment was determined using ImageJ software. TIFF images from the Olympus IX81 microscope were opened and a base X axis was set for each image to align with the long axis of the tube. Individual neurite and actin filament alignment was then measured and compared to the base X axis using the line tool. Exactly 100 measurements were made for each sample type.

Neurite length was measured using the freehand line tool in ImageJ. Individual neurites were traced and compiled. If there were multiple neurites per cell then all were measured. If neurites contained branches the length was measured along the longest branch.

3.4 RESULTS

3.4.1 Fabrication of virus substrates

Virus alignment was achieved on the concave surface of capillary tubes through a flow based assembly method. After this general method was set up, three variables were determined to have significant affects on final virus substrates: surface properties, flow rate, and virus concentration. Each of these variables was investigated separately before final substrates were made for cell experiments.

Virus alignment was achieved on the concave surface of capillary tubes through a flow based assembly method (Figure 3.1). For this method a polypropylene feeder tube (inner diameter 0.16 cm) was attached to a glass capillary (inner diameter 0.15 cm). The glass capillary had been previously coated with chitosan. Then a solution of virus was

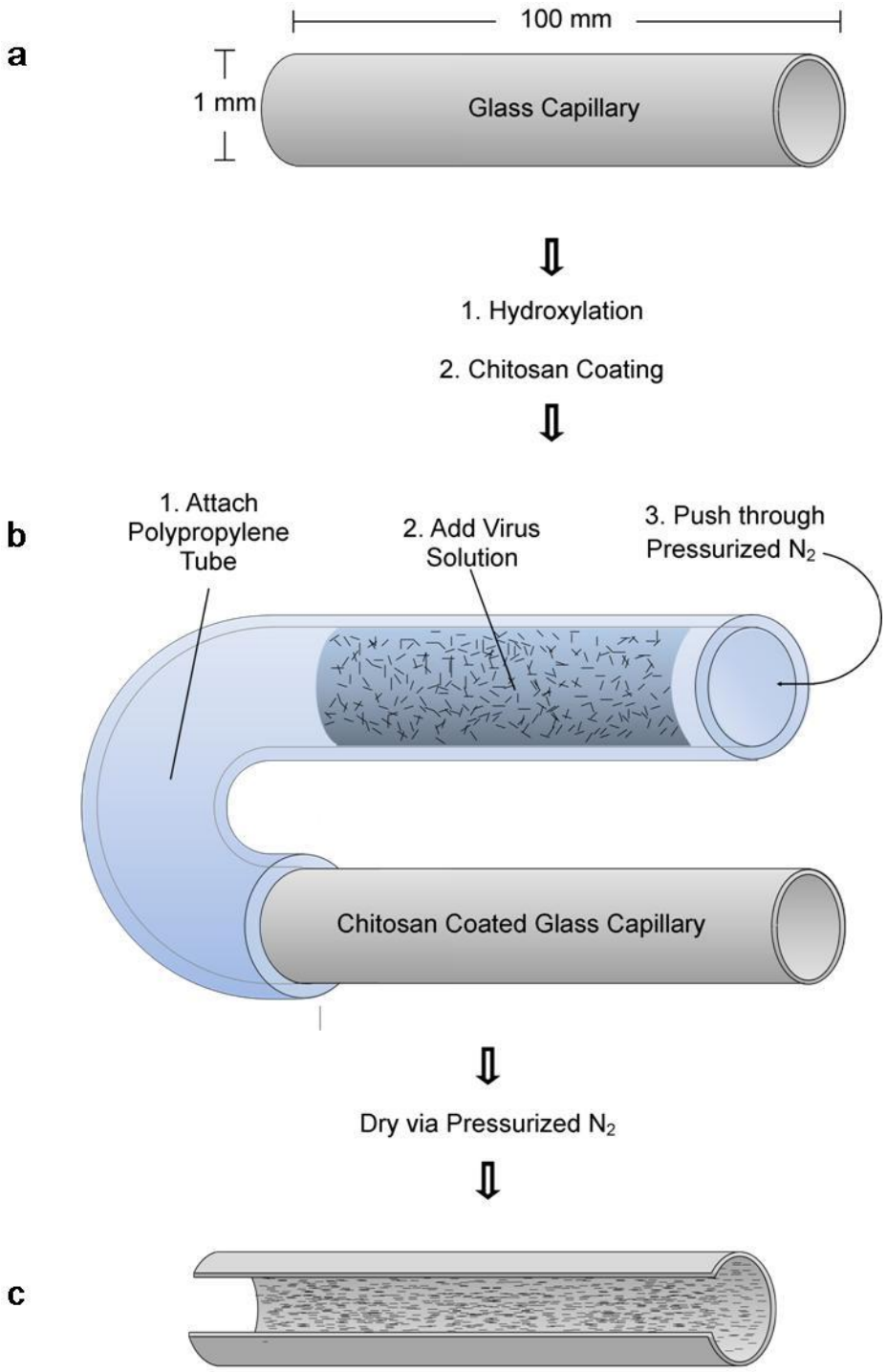

Figure 1.1 Schematic illustration of the fabrication process. a) Glass capillaries were coated with chitosan. b) Virus solution was driven from feeder tube through capillaries at a fluid flow rate of ~200cm·s^{-1}. c) Capillaries were dried using pressurized N2. Internal surface of glass capillaries had TMV particles deposited evenly with an overall orientation along the long axis of the capillary or direction of flow.

added to and held in the feeder tube. The other end of the feeder tube was connected to a high pressure N_2 cylinder. Finally the virus solution was forced, via pressure, out of the polypropylene feeder tube and through the surfaced modified glass capillary into a waste unit. The N_2 gas was kept on until the glass capillary was completely dried.

Through preliminary experiments it was found that surface properties of the glass capillary tubes played an important role in forming the aligned virus structure. Surface energy and charge distribution were critical. Aligned virus structures could only be formed on positively charged surfaces. To create a uniform positively charged surface, capillary tubes were coated with cationic compounds i.e. poly(diallyldimethylammonium chloride) (PDDA), (3-aminopropyl)triehoxysilane (APTES), or chitosan. However, all cell work was done on chitosan because it was found to be nontoxic to the cells.

Alignment of virus particles depended significantly on N_2 flow rate. Shear force created by the flow aligned the virus particles. When no fluid flow was applied only random virus was observed. Different flow rates were tried (50 to 200 $cm \cdot s^{-1}$) with a fixed concentration of TMV (0.015 $mg \cdot mL^{-1}$). The angular spread distribution of TMV for each of the flow rates was obtained. With increased flow rate the width of the angular distribution narrowed. The best alignment was found to be 200 $cm \cdot s^{-1}$. With this flow rate 84% TMV particles were aligned within $\pm 10^{\circ}$.Thus this flow rate was used for all materials used in cell experiments.

Virus concentration was varied to control the density of virus particles on glass capillary tubes. TMV concentration was varied from 0.002 to 0.05 $mg \cdot mL^{-1}$. For these concentrations coverage varied from 50% to 95%. Also, at higher concentrations better alignment was observed, which has been observed in other systems [105]. It was

important to create RGD1 mutant substrates that had virus surface densities similar to TMV substrates. However it was found that much higher concentrations of RGD1 were needed to create similar densities to TMV. RGD1 substrates were coated at 0.2 $mg \cdot mL^{-1}$. TMV substrates were coated at 0.002 $mg \cdot mL^{-1}$ (Figure 3.2).

Substrates for cell experiments were made to have either aligned or unaligned virus particles. Specifically, four types of substrates were made: unaligned TMV, aligned TMV, unaligned RGD1, and aligned RGD1 (Figure 3.2). Once these unaligned and aligned substrates were made, the orientation of virus particles on these substrates was quantified by measuring the incident angle of 100 individual virus particles. For all samples the abscissa was set parallel with the flow direction, i.e. the long axis of the tube. The angular spread distribution of virus particles for each of these substrates is shown in Figure 3.3. There is not any significant alignment of virus particles in either the unaligned RGD1 or unaligned TMV samples. But there is significant alignment of virus particles in both the aligned RGD1 and aligned TMV samples.

A second set of substrates was made for cell experiments. These substrates had either low or high virus density. Four substrates were made: low RGD1 aligned, high RGD1 aligned, low TMV aligned, and high TMV aligned (Figure 3.4). As mentioned before the deposition of RGD1 was lower than that of TMV when identical concentrations were used. This was accounted for by using different concentrations for each type of virus. Low RGD1 aligned and high RGD1 aligned substrates were made from 0.02 $mg \cdot mL^{-1}$

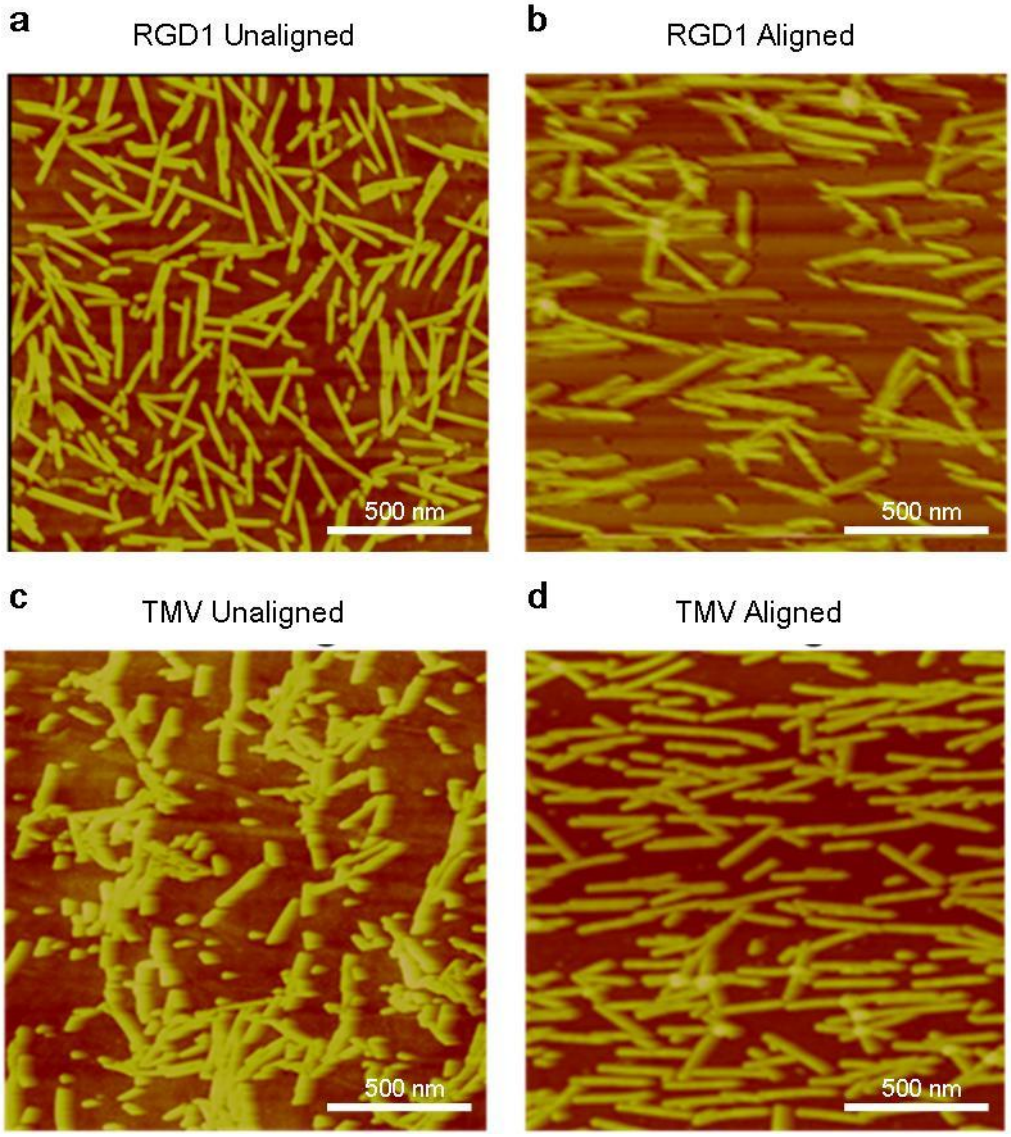

Figure 3.2 AFM images of unaligned and aligned virus substrates. (**a**) Unaligned RGD1 mutant, 0.2 mg·mL^{-1}. (**b**) Aligned RGD1 mutant, 0.2 mg·mL^{-1}, coated on chitosan tube. (**c**) Unaligned TMV substrate 0.002 mg·mL^{-1}. (**d**) Aligned TMV substrate, 0.002 mg·mL^{-1}, coated on chitosan tube.

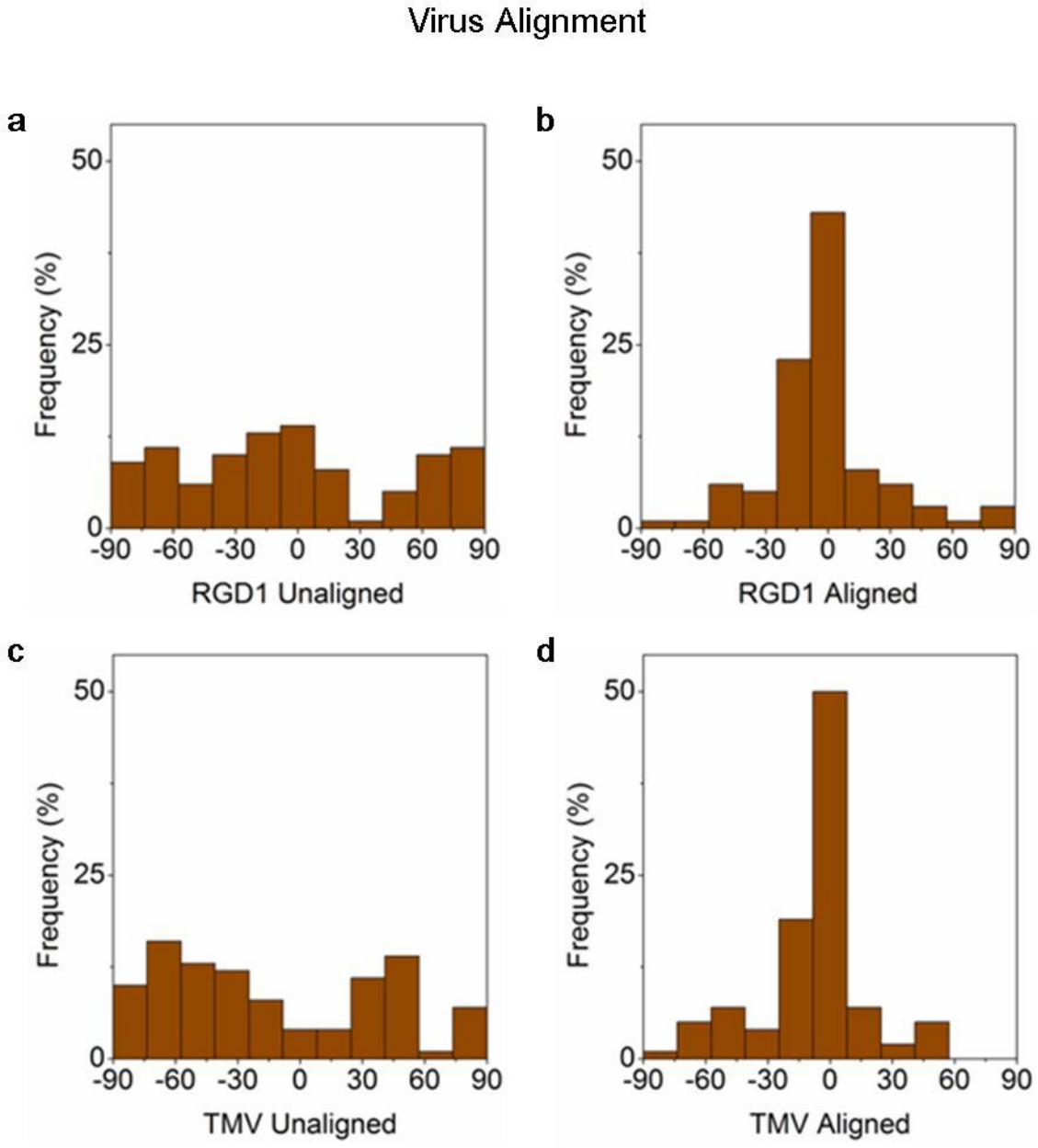

Figure 3.3 Distribution of virus particle orientation for unaligned and aligned virus substrates. (**a**) Unaligned RGD1 mutant, 200 µg/mL. (**b**) Aligned RGD1 mutant, 200 µg/mL, coated on chitosan tube. (**c**) Unaligned TMV substrate, 2 µg/mL. (**d**) Aligned TMV substrate, 2 µg/mL, coated on chitosan tube.

and 0.2 mg·mL^{-1} RGD1 solutions. Low TMV aligned and high TMV aligned substrates were made from 0.002 mg·mL^{-1} and 0.02 mg·mL^{-1} TMV solutions (Figure 3.4). Once these low and high density aligned substrates were made the orientation of virus particles on these substrates was quantified. The angular spread distribution of virus particles for each of these substrates can be seen in Figure 3.5. In this figure we can see that there was alignment of virus particles on all of the substrates.

3.4.2 Myoblast response to virus alignment and density.

Myoblast cells were grown on unaligned and aligned virus substrates for 10 days. During this time cell attachment and spreading was monitored. It was found that myoblasts attached and spread on all substrates by 24 hours. By day 7 myoblasts were confluent on all substrates but no alignment was observed for any of the samples. On day 10 myoblasts began to come off of substrates.

To determine the affect of virus density, myoblast cells were grown on low and high density aligned virus substrates for seven days (Figure 3.4). Again, cell attachment and spreading was monitored. After 24 hours myoblasts had attached to all substrates with no difference between low density and high density virus coatings. As myoblasts continued to proliferate alignment was seen on the high density TMV substrates but not on low density TMV or RGD1 virus substrates.

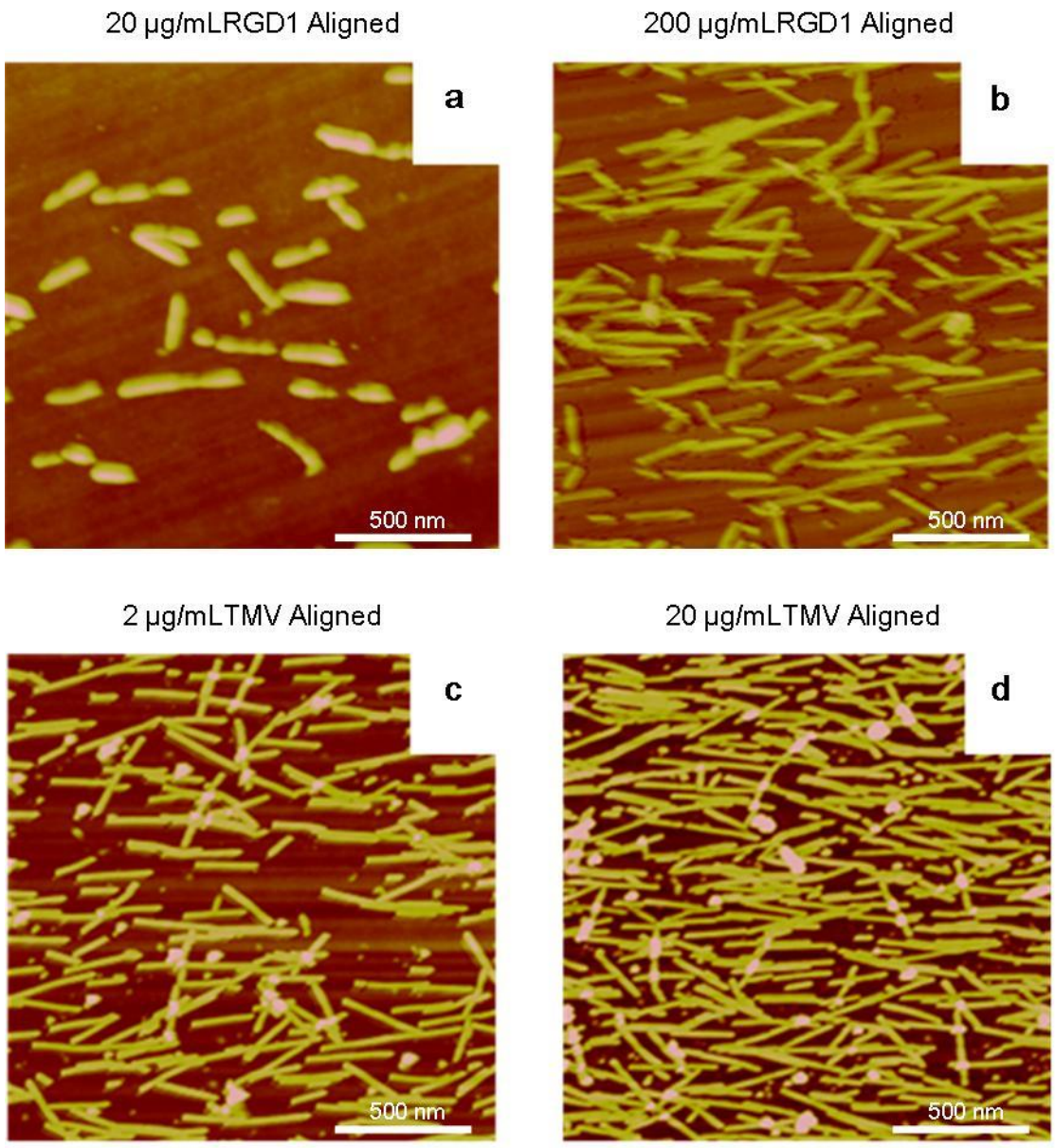

Figure 3.4 AFM images of virus particles in chitosan coated tubes. (**a**) Low density RGD1 mutant, 0.02 mg·mL^{-1}, coated on chitosan tube. (**b**) High density RGD1 mutant, 0.2 mg·mL^{-1}, coated on chitosan tube. (**c**) Low density TMV, 0.002 mg·mL^{-1}, coated on chitosan tube. (**d**) High density TMV, 0.02 mg·mL^{-1}, coated on chitosan tube.

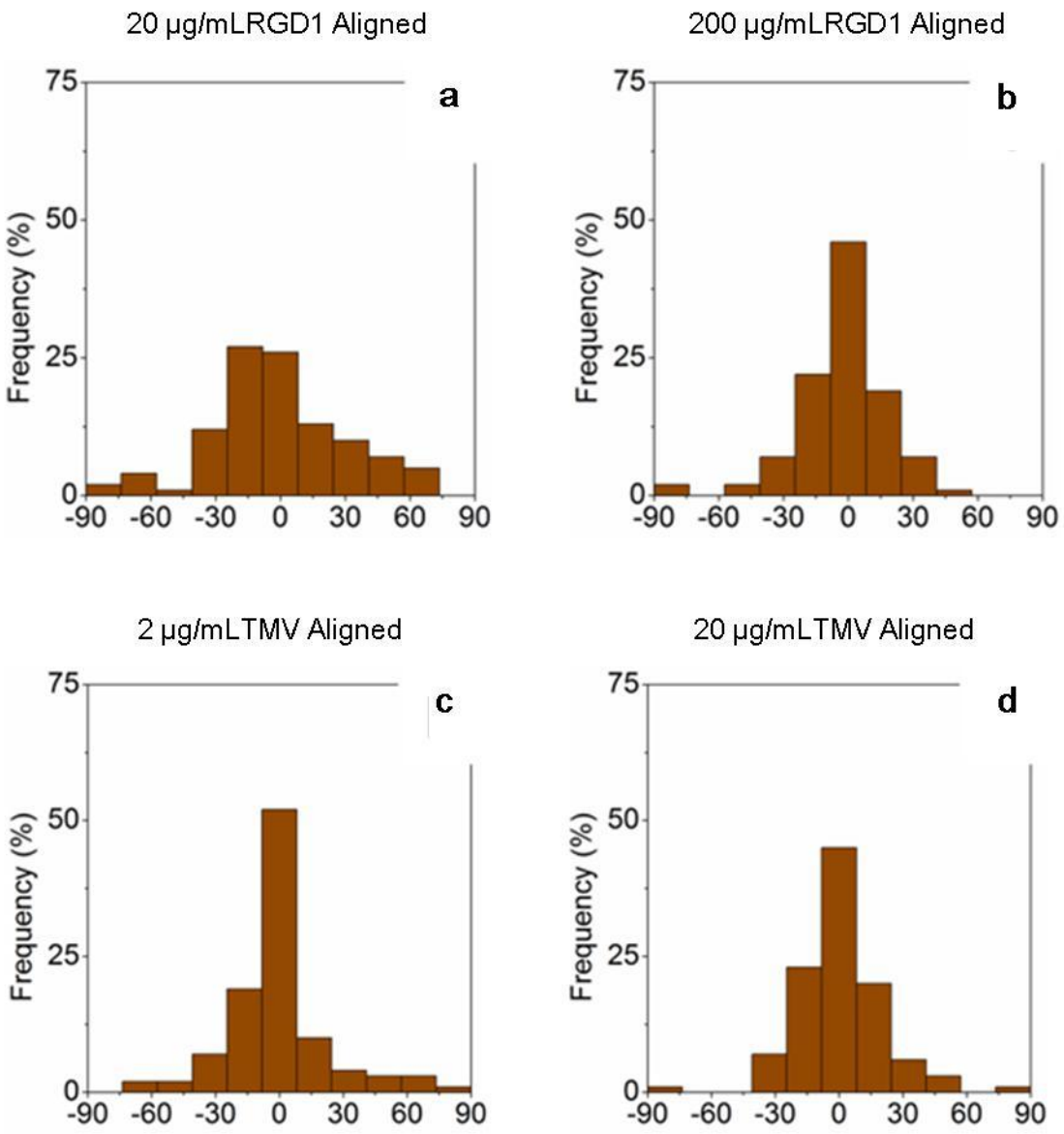

Figure 3.5 Distribution of virus particle orientation on chitosan tubes. (**a**) Low density RGD1 mutant, 0.02 mg·mL^{-1}; (**b**) high density RGD1 mutant, 0.2 mg·mL^{-1}; (**c**) Low density TMV, 0.002 mg·mL^{-1}; and (**d**) High density TMV, 0.02 mg·mL^{-1}.

3.4.3 Myoblast alignment and differentiation on native virus substrates.

Myoblast alignment was observed on high density TMV aligned substrates by day seven. At this point myoblasts were fixed and stained with rohdamine conjugated phalloidin and DAPI. Cells were then imaged using a fluorescent microscope. Images showed the actin filaments of myoblasts on high density TMV aligned substrates were aligning (Figure 3.6). To quantify this alignment the incident angle of individual actin filaments was measured in each sample type. For all samples the abscissa was set parallel with the tube. This corresponded with the known direction of virus alignment. As shown in Figure 3.7, the alignment of actin filaments is significantly increased on the high density TMV aligned substrates. Furthermore, by day 7 myotube formation was observed on high density TMV aligned substrates. When these samples were stained for actin (rohdamine-phalloidin), it was noted that actin expression in these myotubes was significantly increased as compared to the rest of the population of myoblasts and compared to the myoblasts on other substrates (Figure 3.6 b). This indicated that myoblasts on high density TMV aligned substrates were entering differentiation sooner than on other substrates. It should be noted that this was without the addition of differentiation medium. By day 8 myoblast sheets began to peel off of the substrates.

Other groups have used materials (grooves) and achieved significant alignment of C2C12 myoblasts [93, 106]. However these studies did not see a change in differentiation. Furthermore, reported studies used coatings of either fibronectin or RGD ligands to enhance myoblast attachment [107, 108]. We found similar results when our RGD1 virus substrates were

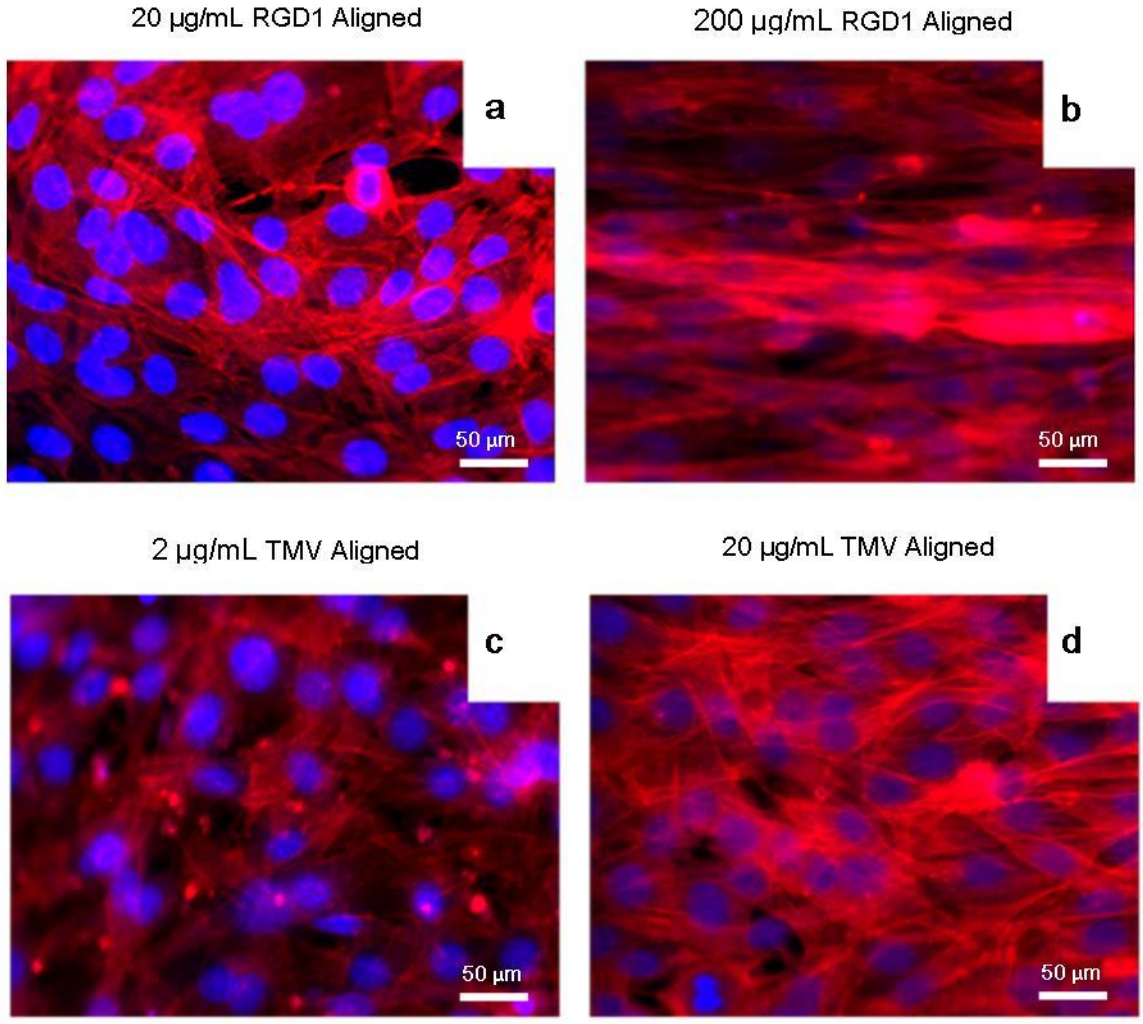

Figure 3.6 Myobalst response to virus substrates. Myoblasts exhibit no alignment on (**a**) low density RGD1 mutant, 0.02 mg·mL^{-1}; (**b**) high density RGD1 mutant, 0.2 mg·mL^{-1}; (**c**) or low density TMV, 0.002 mg·mL^{-1}.and (**d**) Myoblasts on high density TMV, 0.02 mg·mL^{-1} exhibit alignment and myotube formation. Nuclei are stained blue by DAPI and actin filaments are stained red by phalloidin-rhodamine.

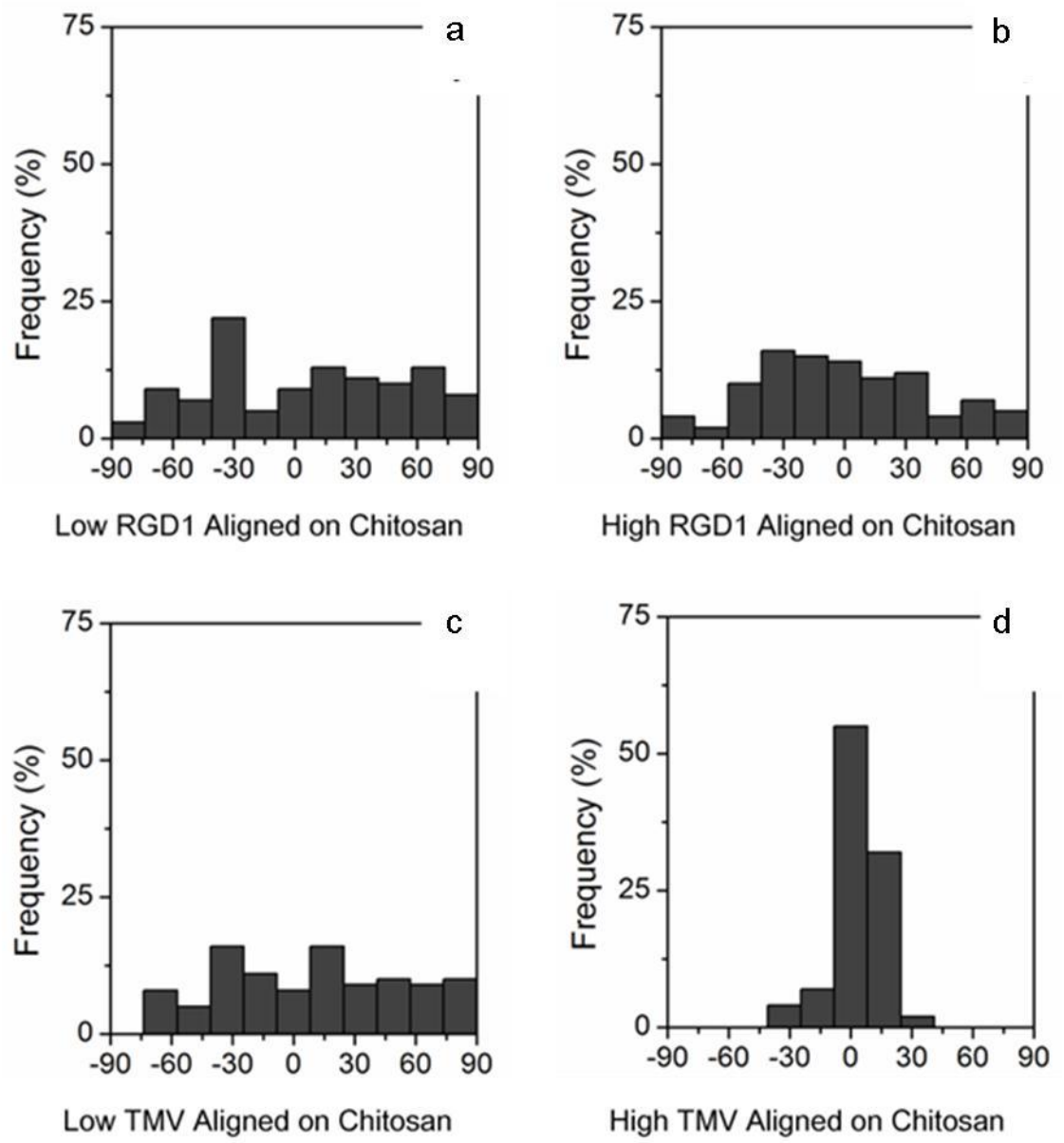

Figure 3.7 Alignment of actin fibers in myoblasts on virus coated chitosan tubes. There is no discernible alignment on (**a**) low density RGD1 mutant coated tubes, (**b**) high density RGD1 mutant coated tubes, or (**c**) low density TMV coated tubes. However, (**d**) on high density TMV coated tubes actin filament alignment is observed which is parallel to underlying virus alignment.

used. This may be due the fact that use of fibronectin as a substrate coating induces hypertrophy in cardiomyocites [109].

3.4.4 Neuroblast response to virus alignment.

Neuroblast cells were seeded on unaligned and aligned virus substrates and observed for 3 days (Figure 3.8). To induce differentiation neuroblasts were seeded and cultured in serum free media. Attachment of neuroblasts and extension of neurites was monitored for 3 days. Neuroblast attachment was observed at 24 hours on all substrates. By day 3 neurite extensions were noticeable on all substrates. Neuroblasts on both unaligned and aligned RGD1 virus substrates had longer neurites than neuroblasts on TMV substrates. These neurites also appeared to be more numerous on the RGD substrates than on the TMV substrates. Alignment of these neurite extensions was quantified. The incident angle of 100 individual neurites was measured in each sample type. For all samples the abscissa was set parallel with the tube to correspond with the known direction of virus alignment. However, there was no significant difference in alignment of neurite extensions on any of the substrates (Figure 3.9).

As mentioned the number of neurite extensions from neuroblasts on RGD1 substrates appeared to be larger than that of neuroblasts on TMV substrates. To quantify this neuroblasts with neurite extensions and neuroblasts without extensions were counted in all samples. It was found that the percentage of neuroblasts with neurite extensions on RGD1 substrates were triple that of the neuroblasts on TMV substrates or the fibronectin control substrates (Figure 3.10).

As mentioned, neurite extensions from neuroblasts on RGD1 substrates appeared to be longer than neurites from neuroblasts on TMV and hFN substrates. To quantify this,

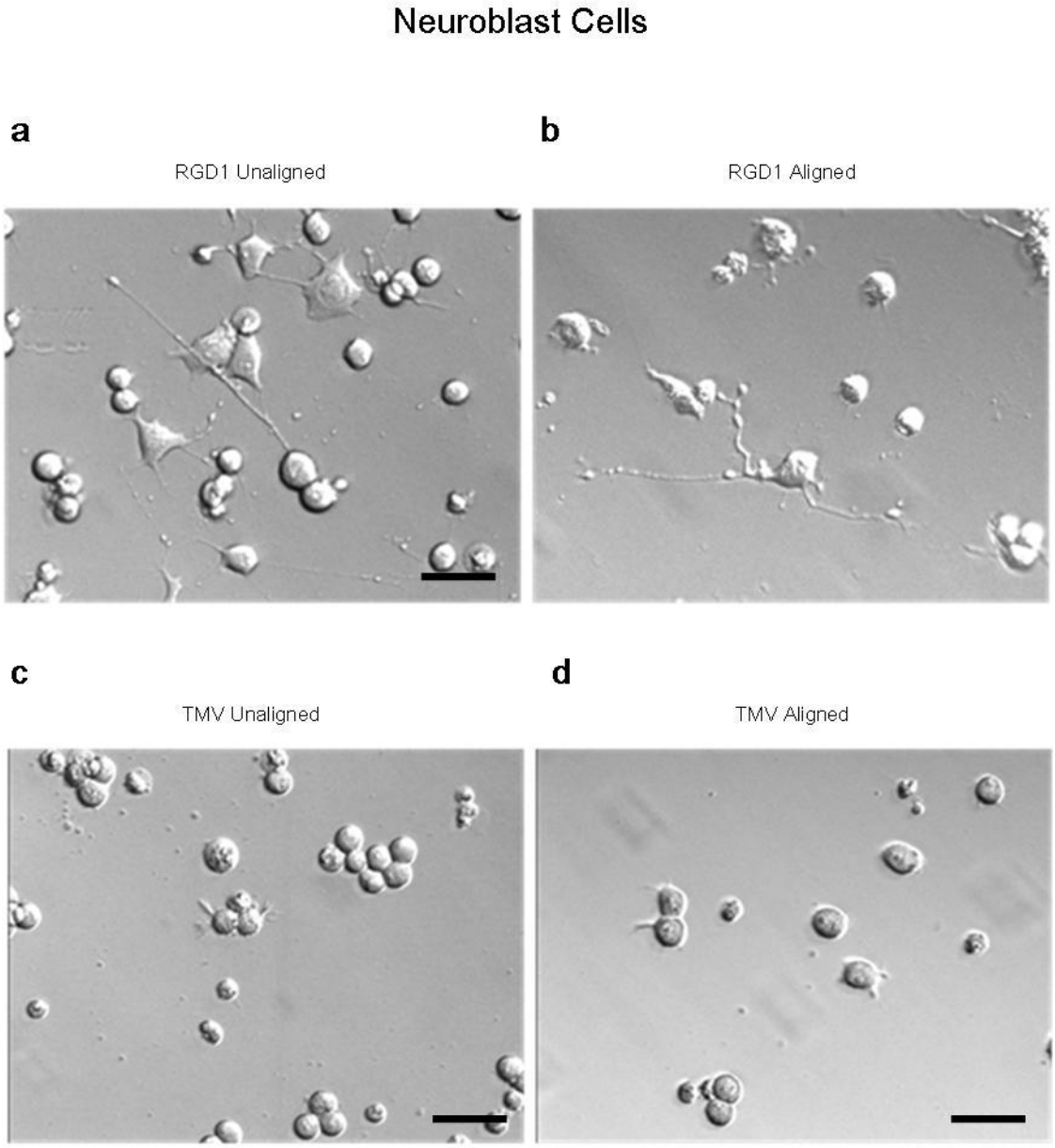

Figure 3.8 Neuroblast response to unaligned and aligned virus substrates. Neuroblasts exhibit neurite extensions on both **a**) unaligned RGD1 and **b**) aligned RGD1 substrates. However, neuroblasts on **c**) unaligned TMV and **d**) aligned TMV substrates exhibit little or no neurite extensions. Neurite extensions are an indication of differentiation. Scale bars are 50 μm.

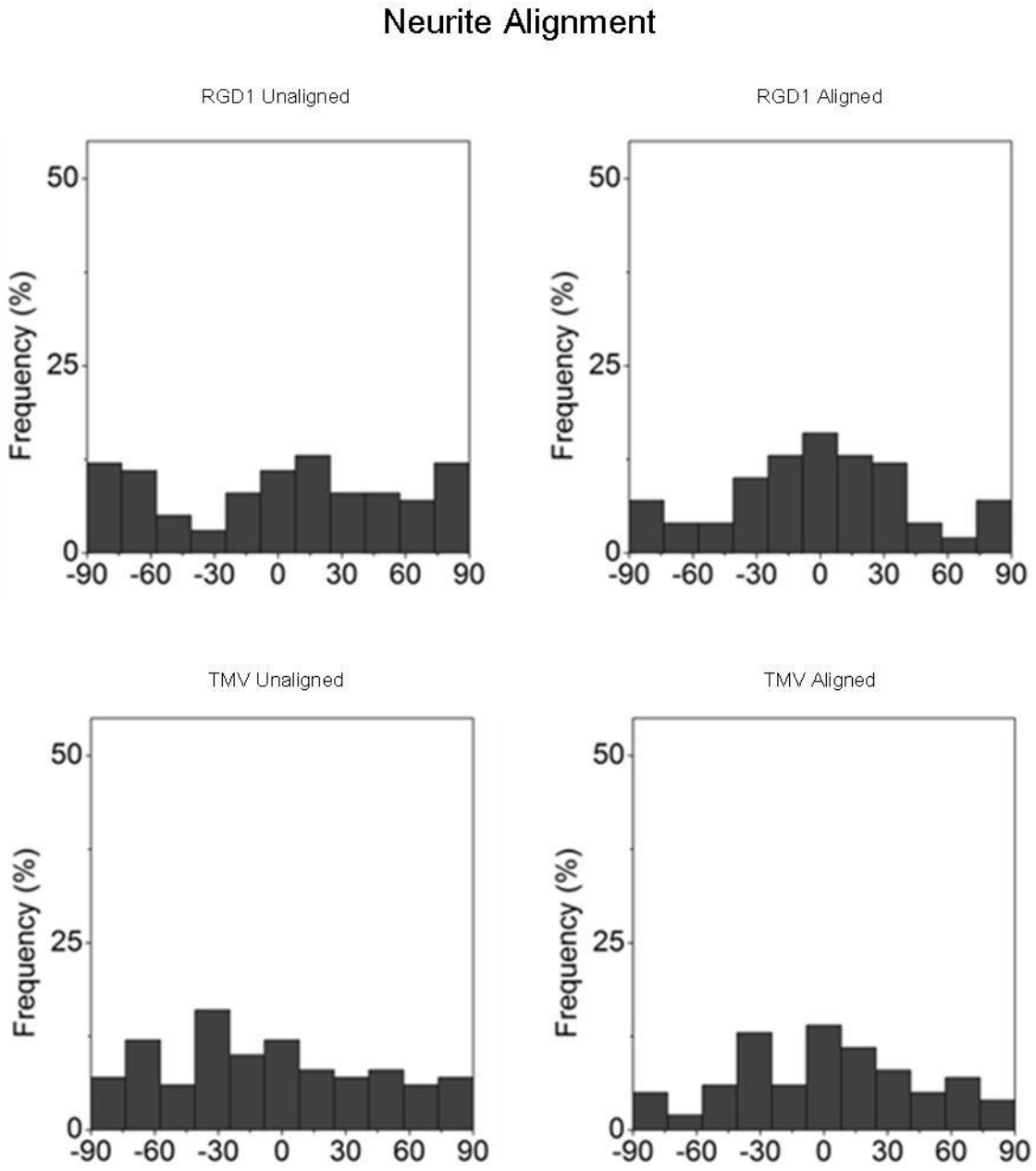

Figure 3.9 Alignment of neurites from neuroblasts on unaligned and aligned virus substrates. There is no discernible alignment on any of the virus substrates.

individual neurite lengths were measured in all samples. It was found that neurite length on RGD1 substrates was triple that of neurites on TMV or hFN substrates (Figure 3.10). Furthermore, there was a significant difference in neurite length between the aligned and unaligned RGD1 substrates. Aligned RGD1 substrates had neurites 20 μm longer than neurites on unaligned RGD1 substrates. Neurite length is often considered a marker of neuronal differentiation. Therefore, these results may indicate that RGD1 virus alignment affects the differentiation of neuroblast cells.

3.5 CONCLUSION

In this chapter, TMV and RGD1 virus mutant particles were aligned on the internal surface of glass capillary tubes. These substrates were then used to align myoblast cells and increase neurite outgrowth in neuroblast cells. Virus alignment and coverage was controlled using flow rate, virus concentration, and surface properties. Myoblast and neuroblast cells attached and grew on aligned and unaligned virus substrates. It was found that myoblast actin filaments aligned with the underlying virus substrates. Furthermore myoblast, cells grown on TMV (0.02 $mg \cdot mL^{-1}$) aligned virus substrates exhibited myotube formation while myoblasts on other virus substrates did not. Neuroblast cells grown on RGD1 virus substrates had increased neurite extensions. However, these extensions did not align with the underlying virus substrates. Nevertheless, virus alignment did significantly affect the length of neurite extensions.

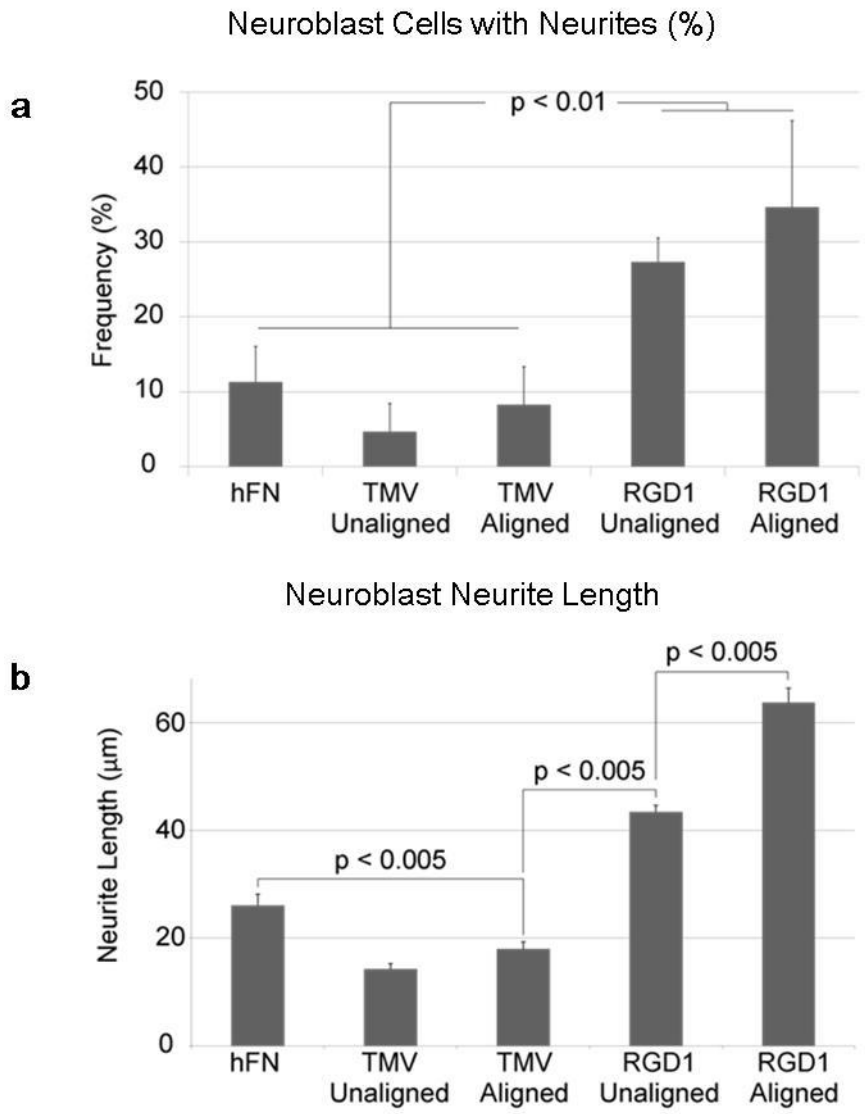

Figure 3.10 Percentage of neuroblasts with neurites and neurite length on unaligned and aligned virus substrates. **a**) Neuroblasts exhibit three times as many neurite extensions on both unaligned and aligned RGD1 substrates than on the TMV or hFN (fibronectin) control substrates. **b**) Neurite length is also considerably increased on the RGD1 substrates as compared to the TMV or hFN control substrates. Furthermore, there is a significant difference in neurite length between the unaligned and aligned RGD1 substrates.

REFERENCES

1. Singh, P., M.J. Gonzalez, and M. Manchester, *Viruses and their uses in nanotechnology.* Drug Development Research, 2006. **67**(1): p. 23-41.
2. Destito, G., et al., *Folic acid-mediated targeting of cowpea mosaic virus particles to tumor cells.* Chemistry & Biology, 2007. **14**(10): p. 1152-1162.
3. Mammen, M., S.-K. Choi, and G.M. Whitesides, *Polyvalent interactions in biological systems: Implications for design and use of multivalent ligands and inhibitors.* Angewandte Chemie International Edition, 1998. **37**: p. 2754-2794.
4. Lee, L.A. and Q. Wang, *Adaptations of nanoscale viruses and other protein cages for medical applications.* Nanomedicine, 2006. **2**(3): p. 137-49.
5. Douglas, T. and M. Young, *Viruses: Making friends with old foes.* Science, 2006. **312**(5775): p. 873-875.
6. Douglas, T. and M. Young, *Host-guest encapsulation of materials by assembled virus protein cages.* Nature, 1998. **393**(6681): p. 152-155.
7. Barnhill, H.N., et al., *Prototype protein assembly as scaffold for time-resolved fluoroimmuno assays.* Journal of the American Chemical Society, 2007. **129**(25): p. 7799-7806.
8. Lee, S.Y., et al., *Deposition of platinum clusters on surface-modified tobacco mosaic virus.* Journal of Nanoscience and Nanotechnology, 2006. **6**(4): p. 974-981.
9. Slocik, J.M., et al., *Viral templates for gold nanoparticle synthesis.* Journal of Materials Chemistry, 2005. **15**(7): p. 749-753.
10. Dujardin, E., et al., *Organization of metallic nanoparticles using tobacco mosaic virus templates.* Nano Letters, 2003. **3**(3): p. 413-417.
11. Lee, S.W. and A.M. Belcher, *Virus-based fabrication of micro- and nanofibers using electrospinning.* Nano Letters, 2004. **4**(3): p. 387-390.
12. Prasuhn, D.E., et al., *Viral MRI contrast agents: coordination of Gd by native virions and attachment of Gd complexes by azide-alkyne cycloaddition.* Chemical Communications, 2007(12): p. 1269-1271.
13. Zinkernagel, R.M., *Immunology taught by viruses.* Science, 1996. **271**(5246): p. 173-178.
14. Lee, L.A., et al., *Mutant Plant Viruses with Cell Binding Motifs Provide Differential Adhesion Strengths and Morphologies.* Biomacromolecules, 2012. **13**(2): p. 422-431.
15. Bruckman, M.A., et al., *Surface modification of tobacco mosaic virus with "click" chemistry.* Chembiochem, 2008. **9**(4): p. 519-23.
16. Lee, S.Y., et al., *Coagulation of tobacco mosaic virus in alcohol-water-LiCl solutions.* Journal of Colloid and Interface Science, 2008. **324**(1-2): p. 92-98.

17. Schlick, T.L., et al., *Dual-surface modification of the tobacco mosaic virus.* J Am Chem Soc, 2005. **127**(11): p. 3718-23.
18. Klug, A., *The tobacco mosaic virus particle: structure and assembly.* Philosophical Transactions of the Royal Society of London Series B-Biological Sciences, 1999. **354**(1383): p. 531-535.
19. Burch-Smith, T.M., et al., *Applications and advantages of virus-induced gene silencing for gene function studies in plants.* Plant Journal, 2004. **39**(5): p. 734-746.
20. Scofield, S.R. and R.S. Nelson, *Resources for Virus-Induced Gene Silencing in the Grasses.* Plant Physiology, 2009. **149**(1): p. 152-157.
21. Sarikaya, M., et al., *Molecular biomimetics: nanotechnology through biology.* Nature Materials, 2003. **2**(9): p. 577-585.
22. Falconnet, D., et al., *Surface engineering approaches to micropattern surfaces for cell-based assays.* Biomaterials, 2006. **27**(16): p. 3044-3063.
23. Stevens, M.M. and J.H. George, *Exploring and engineering the cell surface interface.* Science, 2005. **310**(5751): p. 1135-1138.
24. Miller, D.C., et al., *Endothelial and vascular smooth muscle cell function on poly(lactic-co-glycolic acid) with nano-structured surface features.* Biomaterials, 2004. **25**(1): p. 53-61.
25. Arnold, M., et al., *Activation of integrin function by nanopatterned adhesive interfaces.* ChemPhysChem, 2004. **5**(3): p. 383-388.
26. Jungbauer, S., et al., *Cell shape normalization, dendrite orientation, and melanin production of normal and genetically altered (haploinsufficient NF1)-melanocytes by microstructured substrate interactions.* ChemPhysChem, 2004. **5**(1): p. 85-92.
27. Kaur, G., et al., *The promotion of osteoblastic differentiation of rat bone marrow stromal cells by a polyvalent plant mosaic virus.* Biomaterials, 2008. **29**(30): p. 4074-81.
28. Liu, H. and T.J. Webster, *Nanomedicine for implants: A review of studies and necessary experimental tools.* Biomaterials, 2007. **28**(2): p. 354-369.
29. Jager, M., et al., *Significance of nano- and microtopography for cell-surface interactions in orthopaedic implants.* Journal of Biomedicine and Biotechnology, 2007.
30. Yoshida, T. and G.K. Owens, *Molecular determinants of vascular smooth muscle cell diversity.* Circ Res, 2005. **96**(3): p. 280-91.
31. Rensen, S.S., P.A. Doevendans, and G.J. van Eys, *Regulation and characteristics of vascular smooth muscle cell phenotypic diversity.* Neth Heart J, 2007. **15**(3): p. 100-8.
32. Owens, G.K., M.S. Kumar, and B.R. Wamhoff, *Molecular regulation of vascular smooth muscle cell differentiation in development and disease.* Physiological Reviews, 2004. **84**(3): p. 767(35).
33. Steg, P.G., et al., *One-year cardiovascular event rates in outpatients with atherothrombosis.* JAMA, 2007. **297**(11): p. 1197-206.
34. Stegemann, J.P., H. Hong, and R.M. Nerem, *Mechanical, biochemical, and extracellular matrix effects on vascular smooth muscle cell phenotype.* Journal of Applied Physiology, 2005. **98**(6): p. 2321-2327.

35. Cheng, W., et al., *Nanopatterning self-assembled nanoparticle superlattices by moulding microdroplets.* Nat Nano, 2008. **3**(11): p. 682-690.
36. Orlin, D.V. and G. Shalini, *Materials Fabricated by Micro- and Nanoparticle Assembly - The Challenging Path from Science to Engineering.* Advanced Materials, 2009. **21**(19): p. 1897-1905.
37. Deegan, R.D., et al., *Capillary flow as the cause of ring stains from dried liquid drops.* Nature, 1997. **389**(6653): p. 827-829.
38. Deegan, R.D., et al., *Contact line deposits in an evaporating drop.* Physical Review E, 2000. **62**(1): p. 756.
39. Maheshwari, S., et al., *Coupling Between Precipitation and Contact-Line Dynamics: Multiring Stains and Stick-Slip Motion.* Physical Review Letters, 2008. **100**(4): p. 044503-4.
40. Xu, J., et al., *Self-Assembly of Gradient Concentric Rings via Solvent Evaporation from a Capillary Bridge.* Physical Review Letters, 2006. **96**(6): p. 066104-4.
41. Lin, Z. and S. Granick, *Patterns Formed by Droplet Evaporation from a Restricted Geometry.* Journal of the American Chemical Society, 2005. **127**(9): p. 2816-2817.
42. Adachi, E., A.S. Dimitrov, and K. Nagayama, *Stripe Patterns Formed on a Glass Surface during Droplet Evaporation.* Langmuir, 2002. **11**(4): p. 1057-1060.
43. Engel, M., et al., *Thin Film Nanotube Transistors Based on Self-Assembled, Aligned, Semiconducting Carbon Nanotube Arrays.* ACS Nano, 2008. **2**(12): p. 2445-2452.
44. Nie, Z., et al., *Self-assembly of metal-polymer analogues of amphiphilic triblock copolymers.* Nat Mater, 2007. **6**(8): p. 609-614.
45. Richa, S. and S.S. Michael, *Centerline Placement and Alignment of Anisotropic Nanotubes in High Aspect Ratio Cylindrical Droplets of Nanometer Diameter.* Advanced Materials, 2009. **21**(1): p. 60-65.
46. Nakamura, H., et al., *A simple method of self assembled nano-particles deposition on the micro-capillary inner walls and the reactor application for photo-catalytic and enzyme reactions.* Chemical Engineering Journal, 2004. **101**(1-3): p. 261-268.
47. Nam, K.T., et al., *Virus-Enabled Synthesis and Assembly of Nanowires for Lithium Ion Battery Electrodes.* Science, 2006. **312**(5775): p. 885-888.
48. Rong, J., et al., *Oriented cell growth on self-assembled bacteriophage M13 thin films.* Chem Commun (Camb), 2008.
49. Daniel , M.K., R.N. Rajesh , and D.V. Orlin *Rapid Deposition and Long-Range Alignment of Nanocoatings and Arrays of Electrically Conductive Wires from Tobacco Mosaic Virus13.* Small, 2006. **2**(12): p. 1462-1466.
50. Niu, Z., et al., *Biological templated synthesis of water-soluble conductive polymeric nanowires.* Nano Letters, 2007. **7**(12): p. 3729-3733.
51. Kaur, G., et al., *Regulation of osteogenic differentiation of rat bone marrow stromal cells on 2D nanorod substrates.* Biomaterials, 2010. **31**(7): p. 1732-1741.
52. Kaur, G., et al., *The synergistic effects of multivalent ligand display and nanotopography on osteogenic differentiation of rat bone marrow stem cells.* Biomaterials, 2010. **31**(22): p. 5813-5824.

53. Niu, Z., et al., *Assembly of tobacco mosaic virus into fibrous and macroscopic bundled arrays mediated by surface aniline polymerization.* Langmuir, 2007. **23**(12): p. 6719-24.
54. Gerthoffer, W.T., *Mechanisms of vascular smooth muscle cell migration.* Circ Res, 2007. **100**(5): p. 607-21.
55. Liang, C.C., A.Y. Park, and J.L. Guan, *In vitro scratch assay: a convenient and inexpensive method for analysis of cell migration in vitro.* Nature Protocols, 2007. **2**(2): p. 329-333.
56. Hao, H., G. Gabbiani, and M.L. Bochaton-Piallat, *Arterial smooth muscle cell heterogeneity: implications for atherosclerosis and restenosis development.* Arterioscler Thromb Vasc Biol, 2003. **23**(9): p. 1510-20.
57. Shanahan, C.M. and P.L. Weissberg, *Smooth muscle cell heterogeneity - Patterns of gene expression in vascular smooth muscle cells in vitro and in vivo.* Arteriosclerosis Thrombosis and Vascular Biology, 1998. **18**(3): p. 333-338.
58. Smith, M.L., et al., *Display of Peptides on the Surface of Tobacco Mosaic Virus Particles*, in *Plant-Produced Microbial Vaccines*. 2009. p. 13-31.
59. Lee, L.A., et al., *Mutant Plant Viruses with Cell Binding Motifs Provide Differential Adhesion Strengths and Morphologies.* Biomacromolecules, 2011. **13**(2): p. 422-431.
60. Pittenger, M.F., et al., *Multilineage potential of adult human mesenchymal stem cells.* Science, 1999. **284**(5411): p. 143-147.
61. Dennis, J.E., et al., *A quadripotential mesenchymal progenitor cell isolated from the marrow of an adult mouse.* Journal of Bone and Mineral Research, 1999. **14**(5): p. 700-709.
62. Majumdar, M.K., et al., *Phenotypic and functional comparison of cultures of marrow-derived mesenchymal stem cells (MSCs) and stromal cells.* Journal of Cellular Physiology, 1998. **176**(1): p. 57-66.
63. Noth, U., et al., *Anterior cruciate ligament constructs fabricated from human mesenchymal stem cells in a collagen type I hydrogel.* Cytotherapy, 2005. **7**(5): p. 447-455.
64. Kopen, G.C., D.J. Prockop, and D.G. Phinney, *Marrow stromal cells migrate throughout forebrain and cerebellum, and they differentiate into astrocytes after injection into neonatal mouse brains.* Proceedings of the National Academy of Sciences of the United States of America, 1999. **96**(19): p. 10711-10716.
65. Calvert, J.W., et al., *Characterization of osteoblast-like behavior of cultured bone marrow stromal cells on various polymer surfaces.* Journal of Biomedical Materials Research, 2000. **52**(2): p. 279-284.
66. Mackay, A.M., et al., *Chondrogenic differentiation of cultured human mesenchymal stem cells from marrow.* Tissue Engineering, 1998. **4**(4): p. 415-428.
67. Johnstone, B., et al., *In vitro chondrogenesis of bone marrow-derived mesenchymal progenitor cells.* Experimental Cell Research, 1998. **238**(1): p. 265-272.
68. Alhadlaq, A., M. Tang, and J.J. Mao, *Engineered adipose tissue from human mesenchymal stem cells maintains predefined shape and dimension: Implications*

in soft tissue augmentation and reconstruction. Tissue Engineering, 2005. **11**(3-4): p. 556-566.
69. Yamamoto, N., K. Furuya, and K. Hanada, *Progressive development of the osteoblast phenotype during differentiation of osteoprogenitor cells derived from fetal rat calvaria: Model for in vitro bone formation.* Biological & Pharmaceutical Bulletin, 2002. **25**(4): p. 509-515.
70. Zhu, H.B., et al., *Controlled growth and differentiation of MSCs on grooved films assembled from monodisperse biological nanofibers with genetically tunable surface chemistries.* Biomaterials, 2011. **32**(21): p. 4744-4752.
71. Denhardt, D.T. and M. Noda, *Osteopontin expression and function: Role in bone remodeling.* Journal of Cellular Biochemistry, 1998: p. 92-+.
72. Lian, J.B., et al., *Osteocalcin gene promoter: Unlocking the secrets for regulation of osteoblast growth and differentiation.* Journal of Cellular Biochemistry, 1998: p. 62-72.
73. Gundberg, C.M., et al., *OSTEOCALCIN - ISOLATION, CHARACTERIZATION, AND DETECTION.* Methods in Enzymology, 1984. **107**: p. 516-544.
74. Murphy, C.J., et al., *Anisotropic Metal Nanoparticles: Synthesis, Assembly, and Optical Applications.* The Journal of Physical Chemistry B, 2005. **109**(29): p. 13857-13870.
75. Xia, Y.N., et al., *One-dimensional nanostructures: Synthesis, characterization, and applications.* Advanced Materials, 2003. **15**(5): p. 353-389.
76. Hone, J., et al., *Electrical and thermal transport properties of magnetically aligned single walt carbon nanotube films.* Applied Physics Letters, 2000. **77**(5): p. 666-668.
77. Wang, X.B., et al., *Anisotropic electrical transport properties of aligned carbon nanotube films.* Journal of Physical Chemistry B, 2001. **105**(39): p. 9422-9425.
78. Javey, A., et al., *Layer-by-Layer Assembly of Nanowires for Three-Dimensional, Multifunctional Electronics.* Nano Letters, 2007. **7**(3): p. 773-777.
79. Fan, Z., et al., *Wafer-Scale Assembly of Highly Ordered Semiconductor Nanowire Arrays by Contact Printing.* Nano Letters, 2007. **8**(1): p. 20-25.
80. Takahashi, T., et al., *Monolayer Resist for Patterned Contact Printing of Aligned Nanowire Arrays.* Journal of the American Chemical Society, 2009. **131**(6): p. 2102-2103.
81. Harnack, O., et al., *Rectifying behavior of electrically aligned ZnO nanorods.* Nano Letters, 2003. **3**(8): p. 1097-1101.
82. Sun, B.Q. and H. Sirringhaus, *Surface tension and fluid flow driven self-assembly of ordered ZnO nanorod films for high-performance field effect transistors.* Journal of the American Chemical Society, 2006. **128**(50): p. 16231-16237.
83. Huang, Y., et al., *Directed Assembly of One-Dimensional Nanostructures into Functional Networks.* Science, 2001. **291**(5504): p. 630-633.
84. Raez, J., J.G. Moralez, and H. Fenniri, *Long-range flow-induced alignment of self-assembled rosette nanotubes on Si/SiOx and poly(methyl methacrylate)-coated Si/SiOx.* Journal of the American Chemical Society, 2004. **126**(50): p. 16298-16299.
85. Kim, F., et al., *Langmuir-Blodgett nanorod assembly.* Journal of the American Chemical Society, 2001. **123**(18): p. 4360-4361.

86. Heo, K., et al., *Large-Scale Assembly of Silicon Nanowire Network-Based Devices Using Conventional Microfabrication Facilities.* Nano Letters, 2008. **8**(12): p. 4523-4527.
87. Rao, S.G., et al., *Large-scale assembly of carbon nanotubes.* Nature, 2003. **425**(6953): p. 36-37.
88. Li, L.S. and A.P. Alivisatos, *Semiconductor nanorod liquid crystals and their assembly on a substrate.* Advanced Materials, 2003. **15**(5): p. 408-+.
89. Tay, C.Y., et al., *Micro-/Nano-engineered Cellular Responses for Soft Tissue Engineering and Biomedical Applications.* Small, 2011. **7**(10): p. 1361-1378.
90. Chung, W.J., et al., *Biomimetic self-templating supramolecular structures.* Nature, 2011. **478**(7369): p. 364-368.
91. Duan, X.F., et al., *High-performance thin-film transistors using semiconductor nanowires and nanoribbons.* Nature, 2003. **425**(6955): p. 274-278.
92. Choi, J.S., et al., *The influence of electrospun aligned poly(epsilon-caprolactone)/collagen nanofiber meshes on the formation of self-aligned skeletal muscle myotubes.* Biomaterials, 2008. **29**(19): p. 2899-2906.
93. Charest, J.L., A.J. Garcia, and W.P. King, *Myoblast alignment and differentiation on cell culture substrates with microscale topography and model chemistries.* Biomaterials, 2007. **28**(13): p. 2202-2210.
94. Schmidt, C.E. and J.B. Leach, *Neural tissue engineering: Strategies for repair and regeneration.* Annual Review of Biomedical Engineering, 2003. **5**: p. 293-347.
95. McCain, M.L. and K.K. Parker, *Mechanotransduction: the role of mechanical stress, myocyte shape, and cytoskeletal architecture on cardiac function.* Pflugers Archiv-European Journal of Physiology. **462**(1): p. 89-104.
96. Cohn, J.N., et al., *Report of the National Heart, Lung, and Blood Institute Special Emphasis Panel on Heart Failure Research.* Circulation, 1997. **95**(4): p. 766-770.
97. Murry, C.E., H. Reinecke, and L.M. Pabon, *Regeneration gaps - Observations on stem cells and cardiac repair.* Journal of the American College of Cardiology, 2006. **47**(9): p. 1777-1785.
98. Grounds, M.D., et al., *The role of stem cells in skeletal and cardiac muscle repair.* Journal of Histochemistry and Cytochemistry, 2002. **50**(5): p. 589-610.
99. Wagers, A.J. and I.M. Conboy, *Cellular and molecular signatures of muscle regeneration: Current concepts and controversies in adult myogenesis.* Cell, 2005. **122**(5): p. 659-667.
100. Pipes, G.C.T., E.E. Creemers, and E.N. Olson, *The myocardin family of transcriptional coactivators: versatile regulators of cell growth, migration, and myogenesis.* Genes & Development, 2006. **20**(12): p. 1545-1556.
101. Battiston, B., et al., *Nerve repair by means of tubulization: Literature review and personal clinical experience comparing biological and synthetic conduits for sensory nerve repair.* Microsurgery, 2005. **25**(4): p. 258-267.
102. Meek, M.F. and J.H. Coert, *Clinical use of nerve conduits in peripheral-nerve repair: Review of the literature.* Journal of Reconstructive Microsurgery, 2002. **18**(2): p. 97-109.
103. Amoh, Y., et al., *Implanted hair follicle stem cells form Schwann cells that support repair of severed peripheral nerves.* Proceedings of the National

Academy of Sciences of the United States of America, 2005. **102**(49): p. 17734-17738.
104. Chen, C.J., et al., *Transplantation of bone marrow stromal cells for peripheral nerve repair*. Experimental Neurology, 2007. **204**(1): p. 443-453.
105. Lanfer, B., et al., *Aligned fibrillar collagen matrices obtained by shear flow deposition.* Biomaterials, 2008. **29**(28): p. 3888-3895.
106. Wang, P.Y., H. Thissen, and W.B. Tsai, *The roles of RGD and grooved topography in the adhesion, morphology, and differentiation of C2C12 skeletal myoblasts.* Biotechnology and Bioengineering. **109**(8): p. 2104-2115.
107. Boateng, S.Y., et al., *RGD and YIGSR synthetic peptides facilitate cellular adhesion identical to that of laminin and fibronectin but alter the physiology of neonatal cardiac myocytes.* American Journal of Physiology-Cell Physiology, 2005. **288**(1): p. C30-C38.
108. Rowley, J.A. and D.J. Mooney, *Alginate type and RGD density control myoblast phenotype.* Journal of Biomedical Materials Research, 2002. **60**(2): p. 217-223.
109. Ogawa, E., et al., *Outside-in signalling of fibronectin stimulates cardiomyocyte hypertrophy in cultured neonatal rat ventricular myocytes.* Journal of Molecular and Cellular Cardiology, 2000. **32**(5): p. 765-776.